Abstract

Low Impact Development (LID) has emerged as a design approach for stormwater management. Rain gardens and permeable pavements are two promising LID practices that have been gradually implemented in real life. Although their performance has to date been studied individually, the potential of combining them in order to optimize their application has to date not been investigated. This project is the first time a prefabricated rain garden (Alma) and concrete grid pavement (CGP) were implemented as an integrated system. This project aimed to estimate the system's interaction mechanism and establish a conceptual model to predict its performance.

Three critical processes – infiltration, drainage and overflow – were simulated by using the explicit Green-Ampt equation, Darcy's Law and level pool routing. While the calibrations for Alma and CGP were conducted separately, their validation was performed using only one test. A sensitivity analysis was carried out to identify the most sensitive parameter in the model in order to gain a better understanding of its performance and compensate the calibration and validation limitations due to inadequate data. As regarded practical purposes, the model was also used to estimate the capacity of the pilot site.

The performance inconsistency that was noted between the first two experiments might have been due to the growth medium structure needing some time to stabilize, especially after the initial ponding experiences. Therefore, the long-term performance had to be taken into consideration. The proposed model had shown its applicability and adaptability in predicting its hydrological behaviour in different inflow scenarios. The efficiency rate when predicting the ponding water variation during unstable inflow was proved to have an average Nash-Sutcliffe model efficiency coefficient of 0.972. The saturated hydraulic conductivity (k_{sat}) was identified as being the model's dominant parameter; indeed, the saturation drainage in CGP dominated the performance and the capacity of the entire system. An awareness of k_{sat} estimation is therefore required in order to make the simulated results more reliable. This pilot site was assessed to have the capability of managing the runoff from its 120 m^2 catchment during a 10-year, 2-hour storm with a 1.4 climate factor due to its high surface storage. While waterfront expansion and base layer engagement were not considered in this project, both of these factors require further specifications in the future.

The project yielded a certain level of insight into the hydrological mechanisms surrounding rain gardens and CGP as well as their interaction. Some submodules could be easily adapted to other LID practice models.

Sammendrag

Low Impact Development (LID) har dukket opp som en designtilnærming til overvannshåndtering. Regnbed og permeable dekke er to lovende LID-praksiser som gradvis er implementert i virkeligheten. Selv om ytelsen deres tidligere har blitt studert individuelt, har potensialet til å kombinere dem for å optimalisere anvendelsen hittil ikke blitt undersøkt. Dette prosjektet er første gang et prefabrikkert regnbed (Alma) og betonggitterbelegg (CGP) ble implementert som et integrert system. Dette prosjektet hadde til formål å estimere systemets interaksjonsmekanisme og etablere en konseptmodell for å forutsi ytelsen.

Tre kritiske prosesser - infiltrering, drenering og overløp - ble simulert ved å bruke den eksplisitte Green-Ampt-ligningen, Darcy's Law og level pool routing. Mens kalibreringene for Alma og CGP ble gjennomført separat, ble valideringene deres utført ved bruk av en enkelt test. En følsomhetsanalyse ble utført for å identifisere den mest sensitive parameteren i modellen, både for å få bedre forståelse for ytelsen og for å kompensere for kalibrerings- og valideringsbegrensningene på grunn av utilstrekkelige data. Modellen ble også brukt til å estimere kapasiteten til pilotstedet for praktiske formål.

Forskjellen i ytelse som ble observert mellom de to første forsøkene kan ha vært på grunn av vekstmediumstrukturen, som trenger litt tid på å stabilisere seg, spesielt etter de første ponding-eksperimentene. Derfor måtte den langsiktige ytelsen tas i betraktning. Den foreslåtte modellen hadde vist sin anvendelighet og tilpasningsevne ved å forutsi sin hydrologiske oppførsel i forskjellige tilstrømningsscenarier. Effektivitetsraten ved prediksjon av dybdevariasjoner i ponding-vann under ustabil tilførsel, ble vist å ha en gjennomsnittlig NSE på 0.972. Den mettede hydrauliske ledningsevnen (k_{sat}) ble identifisert som modellens dominerende parameter; faktisk dominerte CGPs metningsdrenering ytelsen og kapasiteten til hele systemet. Det kreves derfor en bevissthet om k_{sat}-estimering for å gjøre de simulerte resultatene mer pålitelige. Dette pilotstedet ble vurdert å ha kapasitet til å håndtere avrenningen fra 120 m^2-avløp under en 10-årig, 2-timers storm med en 1.4-klimafaktor på grunn av sin høye overflatelagring. Mens utbygging av vannkanten og grunnlaget ikke ble vurdert i dette prosjektet, krever begge disse faktorene ytterligere spesifikasjoner i fremtiden.

Prosjektet ga et visst nivå av innsikt i de hydrologiske mekanismene rundt regnbed og CGP, samt deres samspill. Noen submoduler kan lett tilpasses til andre LID-praksis-modeller.

Preface

This report is the result of the course "TVM4905 - Water Supply and Wastewater Systems, Master's Thesis" at Norwegian University of Science and Technology (NTNU). The aim of the thesis is to evaluate the hydrologic mechanism of a prefabricated rain garden Alma and its interaction with surrounding concrete grid pavement.

This thesis is a part of the EU project and also contributed to Klima 2050, Centre for Research-based Innovation as a cooperation between NTNU, SINTEF, Storm Aqua. I am very grateful for the opportunity to work within the cooperation between the associations and would like to thank everyone involved in this process.

I would like to thank my supervisor at NTNU, Professor Sveinung Sægrov, for his support and guidance during the semester. I would like to express my deepest gratefulness my co-supervisor Senior Research Scientist Edvard Sivertsen for his engagement throughout the study including tests, model establishment and data analysis. I would like to express my gratefulness to Per Møller-Pedersen for his expertise and conversations, and other employees at Storm Aqua, who built the testing site and gave assistance during the experiments. In addition, I would like to thank Researcher Jardar Lohne for his writing suggestions and my friend Li Li for all the days that we spent together in the computer lab.

Trondheim, June 10, 2019

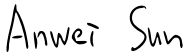

Anwei Sun

Structure

The thesis is paper-based, which is about to be submitted to Urban Water Journal. A manuscript of the paper ("Hydrological modelling of Alma rain garden and concrete grid pavement") is therefore the main content of the thesis. Due to the confidentiality of Alma, the relevant model, results and discussion are presented in the Appendix 1. The complementary information and results not included in the paper are in the Appendix 2-4. The outcome model was established using MATLAB with an Excel as input and the script is in the Appendix 5.

Table of Contents

List of Figures

List of Tables

List of Abbreviations

CGP	Concrete grid pavement
GA	Green-Ampt equation
HEC-HMS	HEC Hydrologic Modelling System
IDF	Intensity Duration Frequency
LID	Low impact development
LPR	Level pool routing
MPD	Modified Philip-Dunne
NSE	Nash-Sutcliffe model efficiency coefficient
SQ	The storage-discharge curve
SWMM	Stormwater Management Model
S3SA	the Stormwater 3-Step Approach

Hydrological modelling of Alma rain garden and concrete grid pavement

Anwei Sun

Department of Civil and Environmental Engineering, Norwegian University of Science and Technology, Trondheim, Norway

This project studied the interactive performance between two Low Impact Development (LID) practices, a prefabricated rain garden (Alma) and concrete grid pavement (CGP). A conceptual model was proposed for the combined system involving three critical processes - infiltration, drainage and overflow - described by the explicit Green-Ampt Model, Darcy's Law and level pool routing. The model's efficacy at capturing the ponding water fluctuation during varying inflow was proved by an average Nash-Sutcliffe model efficiency coefficient of 0.97. The most sensitive parameter was identified as being the saturated hydraulic conductivity. This pilot testing site was found to have the capacity to handle at least a 10-year, 2-hour storm. The project yielded a certain level of insight into the model establishment for rain gardens and CGP as well as their interaction mechanism. Further, the model and submodules could be easily adapted to different scenarios or other types of implementation in order to predict flow release and tailor design.

Keywords: rain garden; concrete grid pavement; interactive hydrological performance; model; stormwater

1 Introduction

Rainfall that has a higher level of intensity and longer duration can be expected in upcoming years due to climate change (Hanssen-Bauer et al. 2015). More stormwater runoff will be generated because of the permeable surface having decreased through urbanization. As a result, stormwater management has become a topic of growing concern. In Norway, a Stormwater 3-Step Approach (S3SA) has been adopted for the entire country: infiltration for light rainfall, attenuation for medium rainfall and guaranteed safe flood paths for heavy rainfall (Lindholm et al. 2008). The practice of low impact development (LID), for instance rain gardens and permeable pavements, has emerged to fulfil the first two steps by reducing impermeable surface area and increasing infiltration and evapotranspiration (Dietz 2007).

A rain garden is a shallow vegetated depression lying on top of an engineered growth medium (Prince George's County 2009; Paus 2016). Previous studies indicate that rain gardens can benefit stormwater volume mitigation, peak flow delay (Davis 2008; Hunt 2008; Li et al. 2009) and stormwater quality improvement by reducing phosphorus, nitrogen, heavy metals, etc. (Davis et al. 2003; Paus 2016; Dietz and Clausen 2005). The performance of traditional rain gardens is dominated by the infiltration capacity of a growth medium while the general indicator saturated hydraulic conductivity (k_{sat}) represents the

theoretical minimum infiltration rate (Paus 2016). It is recommended to have a k_{sat} of at least 10 cm/h (25°C) in order to guarantee its performance in winter (Paus, Muthanna and Braskerud 2016; FAWB 2009) and a suggested maximum drainage time of 48 hours (Lindholm, in Ødegaard et al. 2012; Prince George's County 2009). Several studies have been conducted by observing rain gardens' long-term performance, the results varying among these projects. The infiltration capacity is enhanced or deteriorated after a long period depending on whether or not the generated positive impact from for example roots and soil (Hatt, Fletcher and Deletic 2009; McCallum et al. 2004) outweighs the negative influence from the soil structure deformation due to clogging, compaction, freezing and thawing cycles, etc. (Paus et al. 2014; Moghadas 2016). Besides empirical models (SCS curve number), conceptual models are established for performance comprehension and prediction. Guo and Luu (2015) proposed a surface-subsurface layer model for rain gardens focusing on surface flow and infiltration as well as the base layer. Physical hydrological models such as continuous-simulated HEC-HMS and SWMM have been widely employed to simulate hydrological behaviour (Zhang and Guo 2012). However, discrepancies from reality have been noticed, as the devices' diversity could not be fully addressed by a universal model. Lately, a number of projects have started to combine conceptual and physical models for application optimisation by specifying the mechanism in addition to creating and importing extra function modules accordingly. She and Pang (2010) developed evapotranspiration and infiltration modules in order to contribute to the existing RUNOFF module in EPASWMM5.

Concrete grid pavement (CGP) is one of the alternatives to impervious pavement for parking areas due to its dependable load-bearing capability. It has a higher runoff mitigation capacity compared with permeable interlocking concrete pavement and permeable concrete pavement (Collins, Hunt and Hathaway 2008). CGP comprises concrete pavers, growth medium, bedding, base, subbases and optional geotextile. The growth medium allows for quick percolation, and the coarse material in the base and subbase layers also provide sufficient permeability. The entire storage capacity consists of the voids within the medium and base course, the optional storage tanks and surface storage (if there are curbs present). The clogging problem has been identified as the main reason behind long-term efficiency deterioration, occurring in the surface layer (Kayhanian et al. 2012; Guo and Luu 2015; Brattebo and Booth 2003) and on the optional geotextile due to fine particle capture (Weiss et al. 2019; Imran, Akib and Karim 2013). Surface infiltration is considered to be the limiting factor (Braga, Horst and Traver 2007), while Weiss et al. (2019) have stated that a sufficient amount of water percolation through pavers could be guaranteed by maintenance so that the subgrade permeability will restrict its overall hydrological performance. The mechanism emphasis therefore varies in different design guidelines and simulation programs. For instance, guidelines from Uni-Group USA (Cao, Poduska and Zollinger 1998) focus more on the temporary storage capacity in the base layer and its stability as a conveyance-based facility. Programs like SWMM and HEC-HMS regard the storage capacity in base layers as the main contributor to positive performance, while the program PerviousPave allows free choice for storage components depending on various systems' physical properties (Weiss 2019). In PCSWMMPP, the infiltration rate equals the drainage flow moving out of the surface layer without the involvement of medium retention. In addition, the percolation between the upper saturation zone and the lower unsaturation zone in the base layer is of major interest (James, James and von Langsdorf 2013). A model for the sand-mix base layer lying under rain gardens was studied in the surface and subsurface model by Guo and Luu (2015);

conversely, it contained the upper saturation zone and lower unsaturation zone in the base in accordance with the Green-Ampt (GA) model.

As mentioned previously, infiltration is one of the critical processes for both practices, and is affected by the soil profile (porosity, initial water content, etc.), k_{sat}, ponding depth, etc. (Dingman 2015). The GA model is one of the most commonly used infiltration models, for example EPASWMM (Rossman 2017), especially in homogeneous soil that has a uniform initial moisture distribution. An assumed sharp wetting front divides the soil into a saturated upper zone and unsaturated lower zone; therefore, the water content drops abruptly to the initial moisture level at the front. Various explicit forms have been derived to avoid performing iteration to solve the implicit form. The most accurate representative so far is the one developed by Barry et al. (2005) with an error reading of 0.00005. By contrast, the explicit form provided by Salvucci and Entekhabi (1994) and established for the ponding condition, has a much simpler formula with an error reading of 2%. The GA model has been theoretically explored in different situations. For instance, Chu (1978) used the implicit GA with a time-adjustment approach to model the flux-controlled infiltration after ponding during unsteady rain events. The Salvucci and Entekhabi (1994) form, modified by time-adjustment, is a specific example of infiltration during steady rain, as stated in Dingman (2015). To improve its application during unsteady rainfall, it has to be adapted with respect to varying levels of intensity.

Both practices are promising for stormwater management. In real life, it is quite common to have a regular garden planted alongside parking lots. The potential hydrological interaction here might optimise the gardens' performance if they can be installed properly and function as an integrated system. Hence, the main objective of the research carried out within this context was to gain an understanding of the interaction between rain garden and CGP. Considering there is no consensus in terms of rain garden design, and the average rain garden might not have an explicit and consistent overflow mechanism, a prefabricated Alma rain garden developed by Storm Aqua was chosen for this project. Besides establishing the model for Alma and CGP, the following research questions have been formulated:

- What is the hydrological interaction between Alma and CGP like?
- What is the most sensitive parameter in the model?
- What is the capacity of the proposed system?

2 Case description

The prefabricated Alma rain garden is a combined infiltration and storage unit (Appendix 1) whose flexibility allows it to be easily adapted to different situations. The pilot site was designed to be symmetrical, where Alma is located along one of the CGP borders (Figure 2.1 left). It is located in the city of Sandnes in southwestern Norway, and is constructed by Storm Aqua, having a catchment area of 120 m^2. The Alma was partly covered by vegetation; in addition, its detention chamber was closed during the experiments and could only be emptied by pulling out the plunger on the bottom. The CGP construction followed the manual (Statens Vegvesen 2018) (Figure 2.1 right). The opening within the impermeable concrete pavers was 8x8cm, taking up 54% of the entire CGP area. The same growth medium was used in both practices.

Alma has four overflow weirs of which one serves as the inlet for the whole system. Besides vegetation interception and evapotranspiration, water infiltrates through the growth media and might accumulate on the surface if the infiltration is overcome by the inflow. Part of the infiltrated water is retained in the medium and utilized by plants. When the ponding water level reaches the overflow pipe, the excess water enters the detention chamber through the pipe. If the detention chamber becomes full, the water level will continually rise until it starts to overflow to the CGP. Water expands and gradually accumulates on the CGP surface, where the growth medium has the same infiltration mechanism with Alma. The final outflow weir is 194 mm above the CGP surface.

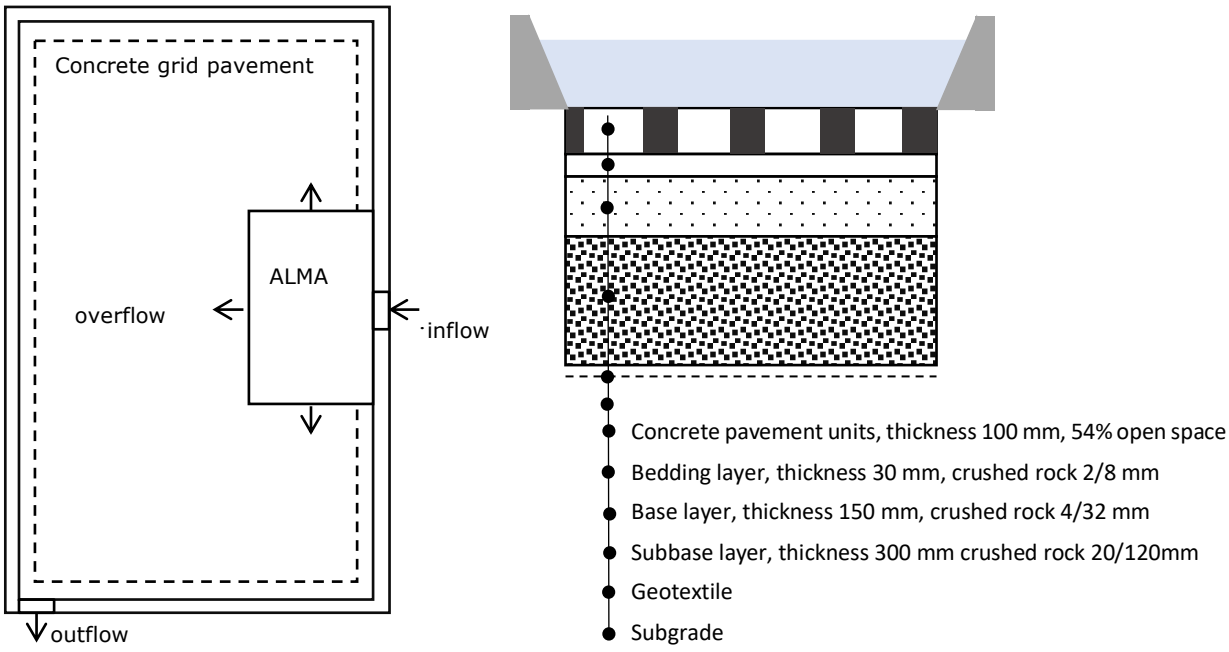

Figure 2.1. The testing site (left) in Sandnes, Norway, where Alma (1480 mm x 880 mm) is surrounded by CGP (2150 mm x 4300 mm) and the structure of CGP (right) is surrounded by curbs having a slope of 30°.

3 Methodology

In order to investigate the hydrological behaviours in the system, a conceptual model was established whose efficiency and ability were tested and verified by experiments and sensitivity analyses.

3.1 Hydrological model

The hydrological processes described in the previous section may be divided into three modules: evapotranspiration, infiltration and overflow. The evaporation in Norway varies from approximately 50 mm/year in mountain areas to 500 mm/year in lower lying areas (Hanssen-Bauer et al. 2009). Due to the short experiment duration and high humidity level during rain events, the evapotranspiration was deemed to be 0 in the model.

Kliewer (2018) has developed a first model for the Alma rain garden focusing on the soil layer's drainage. However, this model did not take into account the overflow process. In order to consider this point, a new model of Alma has been developed, one that recognizes all the processes. Yet due to confidentiality reasons, the finished model, results and discussion related to Alma are presented in Appendix 1. In the following only the interaction between Alma and CGP will be presented along with the details about infiltration and drainage in the CGP.

3.1.1 Infiltration

The total amount of water entering the system has two components - precipitation and runoff from catchment - contributing to the effective hydraulic loading i_e. It was assumed that the water was spontaneously and evenly applied on Alma and the CGP. The slope of the curbs has resulted in a considerable variation in ponding surface along the increase in ponding depth. Hence, the contribution area is defined for each time sequence (Equation 1)

$$i_e(t) = \begin{cases} \frac{P(t)}{void} + \frac{Q_{in}(t)}{A \times void}, & P(t) + \frac{Q_{in}(t)}{A \times void} < k_{sat} < \Delta s(t-1), d_c(t-1) = 0 \\ P(t) + \frac{Q_{in}(t)}{A(d_c)}, & d_c(t-1) > 0 \end{cases} \quad (1)$$

where P is precipitation, void is the CGP open space ratio, Q_{in} is inflow, A is the area of CGP, $A(d_c)$ is the surface area of ponding water, Δs is the water storage deficit and d_c is the ponding depth in the CGP.

The infiltration module has three phases:

(1) Advance of wetting front and unsaturated drainage
(2) Saturation
(3) Recession

Chu (1978) provided an infiltration estimation method during unsteady rainfall using an implicit GA equation and time-adjustment approach, which was modified and expanded upon in this project using the Salvucci and Entekhabi (1994) explicit GA equation. When i_e is less than or equal to k_{sat}, all the water should be infiltrated. Otherwise, the probability of ponding is evaluated by the surface condition indicator for ponding (C_u) (Equation 2). Ponding might occur if C_u is positive and has been assumed to be in the middle of the time sequence since the 1 minute is relatively short. The calculation for the ponding time (t_p) has therefore been simplified compared with the original calculation formula.

$$C_u = \sum_1^t (Q_{in}(t) + P(t)A) - \sum_1^{t-1} Q_d - \frac{k_{sat} \times \psi_f \times \Delta\theta}{i_e - k_{sat}}, \quad i_e - k_{sat} > 0 \quad (2)$$

where ψ_f is suction head assumed to be the same from surface to wetting front, and $\Delta\theta$ is initial soil moisture deficit.

The drainage out of the soil (Q_d) must be subtracted from the cumulative infiltrated water without ponding (F_p) (Equation 3). The estimation for the actual infiltration rate (f_a) and Q_d will be explained later. Since the occurrence of ponding takes place in the middle of a time sequence, the infiltration rate during this 0.5 minute has been assumed to be k_{sat}.

$$F_p(t) = \sum_1^{t_p - 0.5} f_a(t) + 0.5k_{sat} - \sum_1^{t_p - 0.5} Q_d(t) \quad (3)$$

The equations (4-7) for compression time (t_c), effective time (t_e) and infiltration rate (f_{eGA}) were obtained from Dingman (2015) and Salvucci and Entekhabi (1994), including the hydraulic influence of ponding water. In addition, f_{eGA} stands for the potential infiltration rate (Equation 8) before it gets saturated.

$$T(t) = \frac{|\psi_f + d_c(t)| \times \Delta\theta}{k_{sat}} \tag{4}$$

$$t_c(t) = \frac{F_p(t)}{k_{sat}} - T(t) \times ln\left[1 + \frac{F_p(t)}{|\psi_f + d_c(t)| \times \Delta\theta}\right] \tag{5}$$

$$t_e(t) = t - t_p + t_c \tag{6}$$

$$f_{eGA}(t) = k_{sat} \times \left[\frac{\sqrt{2}}{2}\left(\frac{t_e(t)+T(t)}{t_e(t)}\right)^{0,5} + \frac{2}{3} - \frac{\sqrt{2}}{6}\left(\frac{t_e(t)}{t_e(t)+T(t)}\right)^{0,5} - \frac{1-\sqrt{2}}{3}\frac{t_e(t)}{t_e(t)+T(t)}\right] \tag{7}$$

$$f_p(t) = \begin{cases} k_{sat}, & i(t) \le k_{sat} \; and \; d_c(t-1) = 0 \\ f_{eGA}(t), & i(t) > k_{sat} \; or \; d_c(t-1) = 0 \end{cases} \tag{8}$$

The available water on the surface and available space in the soil should create restrictions to f_a. The available surface water consists of the standing water on both the impermeable area and open space. The overall water depth $i_e(t) + d_c(t-1)$ is therefore modified, as presented in Equation 9. The storage deficit is involved in order to fulfil the unsaturation prerequisite. This is due to the fact that in this model the difference between saturated and unsaturated flow is significant; thus, the boundary between saturation and unsaturation has to be clear. As concerns saturation, f_a is equal to the drainage rate estimated by Darcy's equation where the impact of ponding depth needs to be calibrated with ε.

$$f_a(t) = \begin{cases} min\left(\frac{i_e(t)+d_c(t-1)}{void \times 0.8}, f_p(t), \Delta s(t-1) + \frac{Q_d(t)}{H}\right), & \theta < \phi \\ k_{sat}\left(1 + \frac{\epsilon d_c(t)}{H}\right), & \theta = \phi \end{cases} \tag{9}$$

where θ is water content, ϕ is porosity and H is the growth medium depth.

One of the fundamental hypotheses of the Green-Ampt model is that the wetting front's descent is driven by infiltrated water filling up voids with particles. The soil below the wetting front has therefore the same condition as it did initially, and water only drains out when the wetting front reaches the soil layer bottom, indicating that the whole medium becomes saturated. She and Pang (2010) mention that drainage water was observed when θ was between field capacity (θ_{fc}) and ϕ, and this could be regarded as a proportion of water content with two calibration factors β_1 β_2 (Equation 10).

$$Q_d(t) = \begin{cases} \beta_1\left(s(t-1) - s_{fc}\right)^{\beta_2} \times A_{soil}, & \theta_{fc} < \theta < \phi \\ k_{sat}\left(1 + \frac{\varepsilon d_c(t)}{H}\right) \times A_{soil}, & \theta = \phi \end{cases} \tag{10}$$

The infiltration capacity from the bedding layer to the ground varied from 5.5 to 27.2 mm/s in an adjacent site which, although it was constructed along the same guidelines, had been serving as a parking lot for a few years (Trandem 2016). Theoretically speaking, it should be lower than one in a newly built site due to compaction and clogging after long-term performance. As mentioned previously, while each layer in the CGP has the possibility to become the limiting factor, in this project it was assumed that no drainage restrictions were generated from layers lying underneath the surface. The storage and ponding depth have been obtained using equations 11-12.

$$s(t) = min\left(s(t-1) + f_a(t) - \frac{Q_d(t)}{A \times void}, s_{max}\right) \tag{11}$$

$$d(t) = \begin{cases} i_e(t) - f_a(t) - \frac{Q_{overflow}(t)}{A}, & d_c(t-1) = 0 \\ d(t-1) + i_e(t) - \frac{f_a(t) \times A \times void + Q_{overflow}(t)}{A(d_c)}, & d_c(t-1) > 0 \end{cases} \quad (12)$$

where $Q_{overflow}$ is the subsequent overflow to surrounding area.

3.1.2 Overflow and interaction

Three overflow processes exist in the system, into Alma's detention chamber, into the CGP from Alma and the subsequent overflow to surrounding area have been estimated using the level pooling routing method (Chow 2010). The overflow into the CGP starts when ponding depth (d_a) reaches the bottom of the trapezoidal overflow weir. The establishment of a storage-discharge (SQ) curve is presented in Appendix 1. The interaction between Alma and the CGP may be divided into 4 phases:

(1) when d_c is lower than the overflow weir. The overflow from Alma is considered as free flow and only confined by the effective water volume above the threshold (V_e)

$$Q_C(t) = min\left(Q_f(t), V_e(t)\right) \quad (13)$$

where Q_f is the discharge obtained by LPR method (Appendix 1).

(2) when d_c is higher than the threshold, and the distance between the two water levels is gradually decreased. The overflow is negatively affected by the downstream water level. Thus, the calculation procedure is the same with phase 1 but the SQ curve changes for each time sequence, by modifying the discharge (Q_t) from overflow equations (Equations A7-A13 in Appendix 1) using Villenote formula (Equation 14) (Chow 2010).

$$Q_s = Q_f \left(1 - \left(\frac{d_c - h_c}{d_a - h_a}\right)^{1.5}\right)^{0.385} \quad (14)$$

where Q_s is the new discharge applied in the SQ ($Q_s \sim \frac{2S}{\Delta t} + Q_s$) curve, h_a and h_c are the elevation from Alma's surface and the CGP to the overflow weir bottom.

(3) when two water levels get really close, this may be regarded as the starting point for two practices functioning as an entire system; as a result, the two water levels remain the same. Since the detention chamber is closed in Alma and the ground infiltration only exists in the CGP, the overflow from Alma levels out the water level deficit, determined by the mass balance (Equation 15).

$$Q_C(t) = min\left(Q_{in}(t) - A_{alma} \times \frac{Q_{in}(t) - f_a(t) \times A \times void - Q_{overflow}}{A(d_c) + A_{alma}}, V_e(t)\right) \quad (15)$$

where A_{alma} is the area of Alma, Q_{in} is the inflow into Alma.

(4) when the water level descends to the overflow weir, the water level in Alma remains at threshold. Phases 1 and 2 might occur depending on the inflow.

A flow chart describing the complete procedure and the written MATLAB code appear in Appendix 4 and Appendix 5 respectively.

3.2 Tests and Measurement

Four experiments (Table 1) were carried out at the testing site in mid-April and early May. Water was provided by a hose located at the inlet. The hose's maximum flow conveyance capacity (3 l/s) and general precipitation pattern were taken into consideration while designing the inflow pattern. No water (as precipitation) was directly added on top of the two practices. The water levels in Alma and the CGP at both the weir and overflow pipe were measured once per minute using measuring sticks.

k_{sat} was estimated by using a Modified Philip-Dunne (MPD) infiltrometer, which had an inner diameter of 8.6 cm and was capable of covering one opening void; it was sealed on the CGP surface by applying silicon (Appendix 3). The falling head data were processed using the MATLAB code obtained from Paus (2016). The initial moisture, field capacity and porosity of the growth medium were measured in the lab. The suction head were obtained from Kliewer (2018) as 3 mm.

3.3 Calibration and validation

The calibration for CGP model was conducted based on Event 3 and 4; its objectives included α'/α modifying k_{sat} in Alma and CGP respectively, β_1 / β_2 for unsaturated drainage flow, and ε adjusting the ponding impact on saturated flow. Event 2 was used for validation. The level of accuracy was presented by using the Nash-Sutcliffe model efficiency coefficient (NSE). The closer the NSE is to 1, the more accurate the model is. The chosen events for calibration and validation have been summarized in Table 1.

Event	Date	Initial Condition	Estimated parameters	Use
1	2019.4.11	Dry, Alma was empty	$\alpha' C_d$	Calibration
2[2]	2019.5.9	Wet, Alma was empty	$\alpha\ \alpha'\ \beta_1\ \beta_2\ \varepsilon$	Validation
3	2019.5.10	Wet, Alma was full	$\alpha\ \beta_1\ \beta_2\ \varepsilon$	Calibration
4	2019.5.10	Wet, Alma was full	$\alpha\ \beta_1\ \beta_2\ \varepsilon$	Calibration

Table 1: A summary of the events used for calibration and validation, indicating the initial condition and estimated parameters

1. α' was estimated for Alma k_{sat}, in this context only α would be discussed for the CGP, while C_d was for overflow estimation.

2. The growth medium in the CGP was retrofitted after Event 1 and became more compacted.

3.4 Sensitivity analysis

Considering the inadequate experimental data, a sensitivity analysis was carried out based on event 3 to identify the influence generated from different parameters, including k_{sat} (α), β_1 / β_2, ε, ψ_f and $\Delta\theta$. The approach was obtained from Rosa et al. (2015) to run the same model after changing only the target parameter to within ±10% and ±50%. The sensitivity of each parameter was assessed using equation 16.

$$sensitivity = \frac{\Delta R}{\Delta P}\ \frac{P}{R} \qquad (16)$$

where ΔR and ΔP are the differences between the original and adjusted results and parameters respectively, and R and P are the original results and parameters respectively. NSE was chosen to be the target model output as R, representing the overall ponding

situation. Hence, a higher positive value of sensitivity indicated a greater negative impact on model accuracy generated by the parameter.

3.5 Practical use

The capacity of this pilot site has been estimated by the proposed model. A design storm with a 10-year return period and 2-hour duration was chosen according to the S3SA definition for second-step facilities to be able to handle stormwater runoff up to 40 mm rainfall (Lindholm et al. 2008). Using the symmetric hyetograph method (Lindholm, in Ødegaard et al. 2012), the rain events were constructed based on the IDF (Intensity Duration Frequency) curve (1974-2015) from Sandnes Municipality (2017), including a recommended climate factor of 1.4. The concentration time was not considered while generating the inflow series. Hence, the inflow was simplified to be the precipitation intensity times area. Regarding the enormous surface storage in the pilot site (194 mm), the height of the outflow weir was reasonably adjusted to be 100 mm above the CGP surface.

3.6 Limitations to the methodical approach

The pilot site is an idealized representative of real life. The symmetrical configuration has a considerable surface storage due to surrounding curbs. Unsaturated flow, waterfront expansion and runoff generation were either simplified or not considered in the model.

4 Results

The physical characteristics of the testing site were investigated through field and lab tests to obtain reliable input for the model. The sensitivity analysis should provide a better understanding of the system's hydrological mechanism. The relevant results are presented in this section.

4.1 Measurement

Although the MPD experiments were conducted 2 hours after event 2 and before event 3 at the same location, it took 20 mins and 7 mins respectively to infiltrate 43cm of water, resulting in a hydraulic gradient of 5 and 20 mm/min. The value of 15.4 mm/min from the first test was applied to the model. The field capacity and porosity of growth medium were 35.4% and 49.4% respectively, in close alignment with the measurement obtained by Kliewer (2018), which was 35.8% and 50% respectively.

4.2 Calibration and Validation

The observed effective water depth and modelled water depth in Alma and the CGP as a function of time for events 3, 4 and 2 are shown in Figure 4.1, Figure 4.2 and Figure 4.4 respectively. The most congruous values for 4 calibration factors are presented in Appendix 2, where a significant inconsistency could be noticed in which α and ε were around 0.73 and 0.54 respectively. The comparison between simulated results using $\alpha, \varepsilon, \beta_1$and β_2 as 0.75, 0.45, 0.68 and 0.80 and observation are presented in Figure 4.1, and Figure 4.2, showing an average NSE of 0.972.

However, all of these options have not been able to make the model result correspond to the observation data for event 2, the first test undertaken after the soil retrofit. By retaining the values of α, $\beta_1$and β_2, ε had to be 1.97 to have an NSE of 0.977 (Figure 4.4).

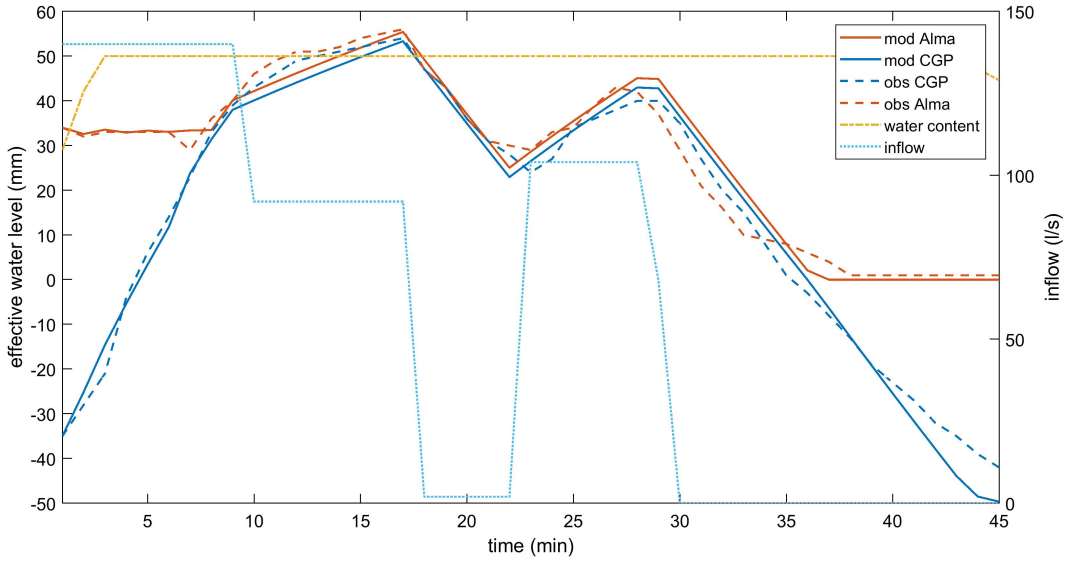

Figure 4.1: The simulated and observed effective water depth, inflow and water content of event 3. Simulated results used calibrated factors α, ε, $\beta_1$and β_2 as 0.75, 0.4, 0.68 and 0.80 respectively.

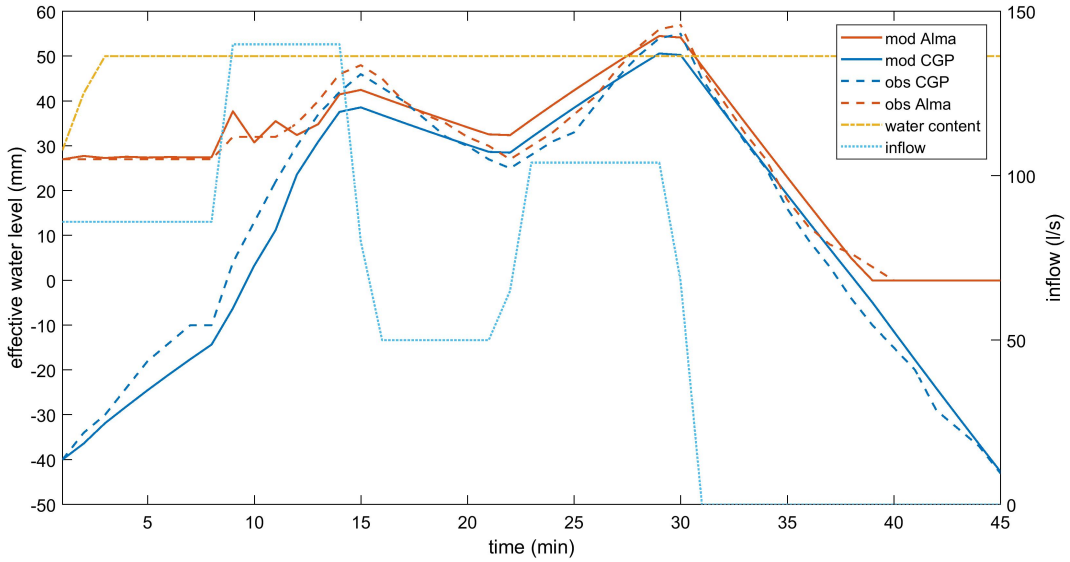

Figure 4.2: The simulated and observed effective water depth, inflow and water content of event 4. Simulated results used calibrated factors α, ε, $\beta_1$and β_2 as 0.75, 0.4, 0.68 and 0.80 respectively.

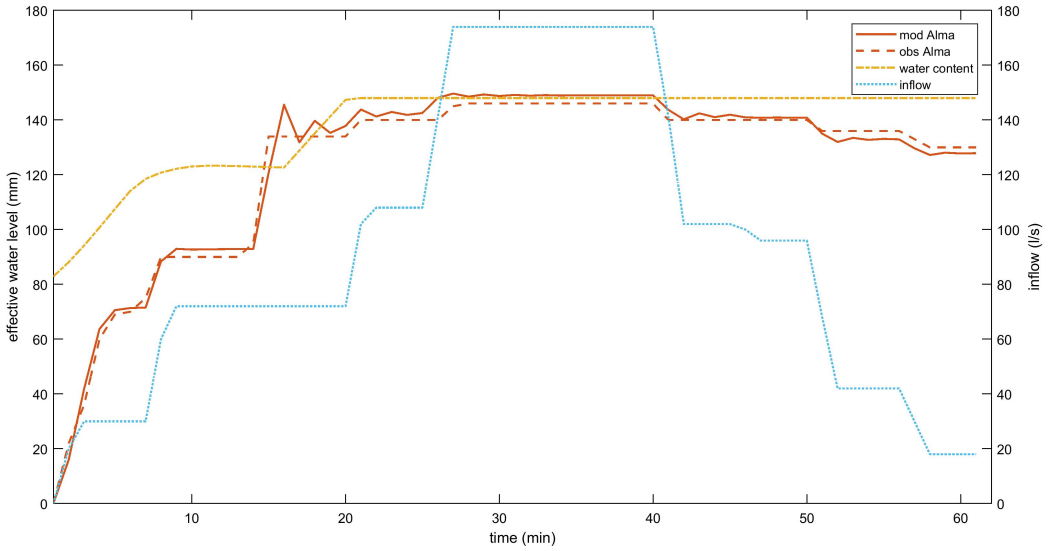

Figure 4.3: The simulated and observed effective water depth, inflow and water content of event 2. Simulated results used calibrated factors α, ε, β_1 and β_2 as 0.75, 1.97, 0.68 and 0.80 respectively.

4.3 Sensitivity analysis

The sensitivity of each parameter is summarized in Table 2. The $k_{sat}(\alpha)$ appeared to be the most sensitive parameter in the model since it had the highest sensitivity of 15.171. The second most sensitive parameter was β_2 as 2.193, followed by ε as 0.679.

Parameter	+10%	-10%	+50%	-50%
α	0.129	0.306	2.095	15.171
β_1	0.020	0.019	0.007	0.160
β_2	0.021	0.018	2.193	0.015
ε	0.021	0.021	0.225	0.679
ψ_f	0.020	-0.001[3]	0.020	0.019
$\Delta\theta$	0.002	0.014	0.013	0.022

Table 2: A summary of the sensitivity results for each parameter, indicating its influence on model efficiency.

[3]The negative value implied 0.9 ψ_f would produce a better NSE.

4.4 Practical use

As shown in Figure 4.4, the design storm is equivalent to 33.3 mm (4287.2 l entering water in total including the catchment area and the whole installation area). The water level rose rapidly as a response to the extreme rainfall peak. The maximum ponding depth was reached before the end of the inflow peak as 114.9 mm. The ponding in the CGP lasted for 36 mins, and the drainage time was estimated to be 27 mins. The total outflow to the surrounding areas was 143.75 l, which was 3.35% of the inflow that the combined system could not handle.

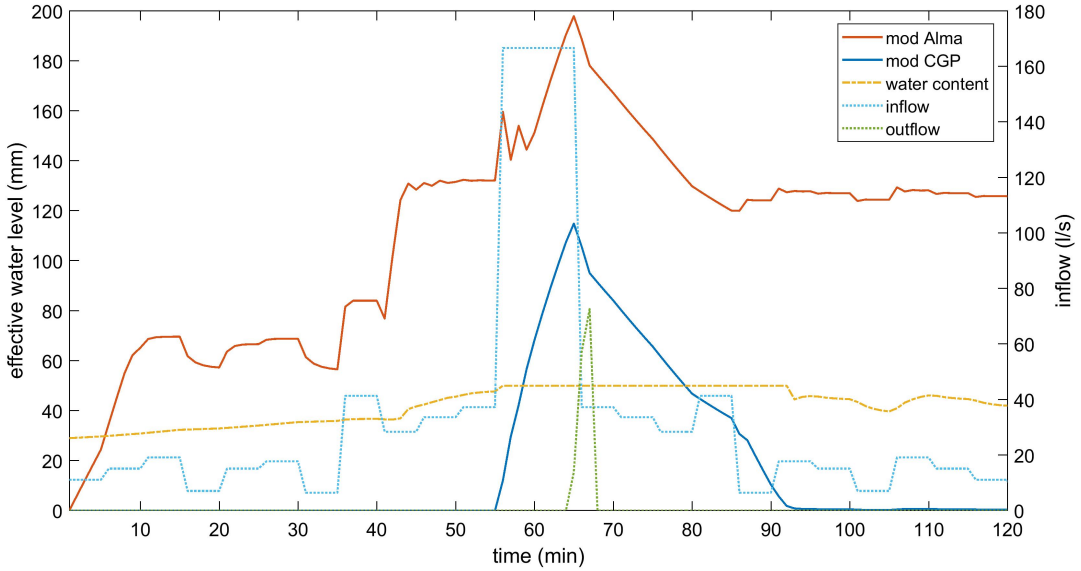

Figure 4.4: The simulated result using a 10-year 2-hour storm with a climate factor 1.4, using calibrated factors α, ε, β_1 and β_2 as 0.75, 0.4, 0.68 and 0.80 respectively.

5 Discussion

This project has made an attempt to investigate the interaction between Alma and CGP, identify the most sensitive parameter in the model and estimate the capacity of the testing site.

5.1 Performance

The calibration results (Figure 4.1 and Figure 4.2) illustrate the ability of the proposed model to capture the water level variation during unsteady inflow. The assumption made for overflow was that the water would spread out instantly, making two water levels stay the same during phase 3. The prerequisite for this to happen was having an adequate overflow capacity to level out inflow and compensate the height difference caused by the ground infiltration in the CGP. The capacity was probably enhanced by the main flow path due to the high-speed inflow (Appendix 3). It was observed that when the water level in the system was high enough, the flow left Alma through the main path but re-entered through the side weirs, causing a full flow circle to occur. The overflow capacity is also of great importance in the descent process; otherwise, two water levels might once again start to be distinguished above the overflow weir.

When it comes to calibration and validation, the decrease in ε from 1.97 to 0.4 implied that ponding water could generate more hydraulic impacts at the very beginning; nonetheless, the medium gradually became more compacted after several ponding tests. The consistent hydrological performance during events 3 and 4 suggests a stable soil profile and the potential physical changes within the medium during event 2, which was the first experiment after the retrofit under approximately 100-mm of standing water. The soil aggregation deformation would also result in a reduction of k_{sat} (Whalley, Matthews and Ferraris 2012), leading to a higher ε than 0.4 for events 3 and 4. Besides the initial

disparity, the influence from clogging and compaction also needs to be accounted for α when considering long-term performance prediction.

Concerning high-speed inflow, the hose was placed at a distance to the inlet in order to mitigate the main flow path and Alma surface disturbance, which, however, resulted in inflow delay and loss. The free inflow was resisted by the existing standing water when its level was higher than the inlet weir. The inflow lag was also due to the control valve's reaction time. The model deficiencies might also be attributed to the random error in ponding measurement enlarged by rapid fluctuation and the varied surface elevation in both Alma and the CGP. It was observed that there was at least a 10-mm difference between the elevation of the middle and edge areas, causing some disparities in Darcy's Law and the GA model with respect to the hydraulic heading.

5.2 Sensitivity analysis

The ability of α and ε to indicate the hydrological performance coincides with the sensitivity they have shown in the model. k_{sat} was identified to be the governing parameter in the GA model under both dry and wet conditions, while ψ_f and $\Delta\theta$ were the second and third sensitive parameters under dry conditions (Parnas 2018). Yet the GA module was a small component in the model assessing the potential infiltration rate for unsaturation. Its administration of infiltration was only valid until the storage deficit started to produce more constraints. According to the water content estimation, the initial unsaturated medium quickly became and remained saturated the most of the time, prioritizing the saturated drainage to become the most dominant process; consequently, this resulted in the overall administration of k_{sat} throughout the entire system. The sensitivity of ψ_f and $\Delta\theta$ was therefore diluted.

The base layer engagement was not included in the model. Guo and Luu (2015) discovered that both the growth medium and base layer would become rapidly saturated and remain full, and the drainage through the underlying pipe was solely governed by Darcy's Law. Due to the unavailable permeability of subgrade and the intermediate investigation into water content, an equilibrium was likely to build up between infiltration and unsaturated flow as a second hypothetical mechanism. This mechanism could be explored more by applying theoretical equations to unsaturated drainage instead of using the simplification seen in this project.

The value of α (0.75) accounting for three events indicates the huge difference between the estimation (15.4 mm/min) and calibration (11.5 mm/min). This inconsistency might originate from the MPD method in both studies. It was required to achieve a minimum hydraulic gradient (i.e., 1 mm/min) to ensure the saturation condition; otherwise, the measured value would be higher than the actual value (Paus, Muthanna and Braskerud 2016), which did not occur in the project (5mm/min). As mentioned, the underlying multilayers not only impeded the percolation but also made it more difficult for soil to become saturated after adding approximately 2.5 l water in one opening (8x8 cm), responding to the soil moisture after test. The estimated α was therefore reasoned to be less than 1.

The limiting experimental data diminished the reliability of the calibration results, making calibration more like a mathematical process, as many options existed to correspond with events 3 and event 4. The chosen values are not necessarily the best to

reflect reality. There was therefore uncertainty regarding the dependability of sensitivity analysis results based on this calibrated model.

5.3 Practical use

Figure 4.4 shows that after 63 mins there was outflow to surrounding areas that lasted for 5 mins (cf. green curve), indicating that this combined system could not handle the complete event. The rainfall obtained by the symmetric hyetograph method had a concentrated intensity distribution (i.e., 13.8 mm in 10 mins), representing an extreme scenario. The abrupt development of ponding depth in the CGP was a response to the dramatic peak. The ponding could be mitigated by enhancing the detention chamber volume through ground infiltration and a drainage pipe.

Moreover, it is not realistic to have a 115mm ponding on the surface, because a parking lot has to be open to the surrounding area. The surface slope could be considered to lead water towards the curbs and enhance the surface storage. On the other hand, doing so would increase the influence from ponding depth variation, and a 2D model would then be required.

While estimating the capacity of LID, it is necessary to take both water quantity and quality control into account. A short drainage time might result in inadequate quality enhancement (Guo and Urbonas 2002). The conclusion has therefore been reached that while this pilot site has had the capability of fulfilling the second-step goal in S3SA, it requires further assessment with respect to pollution retention and practical application.

5.4 Consequences of limitation

As mentioned above, the pilot site did not fully represent reality. If the system had not been symmetrical or had a larger CGP, the expansion would have been of greater concern in the model affected by the overflow rate, infiltration capacity, surface slope, etc. The expansion also sharply increases the spatial difference within the CGP, for example the water content within and outside the waterfront. The consequence of making a 1D model is the deviation of water depth in the CGP at the initial phase of interaction. It would not make a great difference during heavy rainfall.

The multiple ponding times (Chu 1978) and separation points did not occur during the experiment due to the simple inflow pattern. They are more likely to happen when the ground infiltration and drainage pipe are available and the rainfall has more fluctuations, all of which would bring more dynamism to the hydrological behaviours.

6 Conclusion

In this study, a prefabricated Alma rain garden and concrete grid pavement were studied for the first time as an integral unit. The proposed concept model for the pilot site had shown its applicability and adaptability in describing all the hydrological processes, including infiltration, drainage, ponding and overflow, in particular the interaction between two separate practices. Each submodule was proven to be exemplary to a certain extent and could be applied to other LID models.

In this model, k_{sat} was identified as being the governing parameter, and the saturation drainage in the CGP was the dominant process controlling the performance and capacity of the entire system. An awareness of k_{sat} estimation is therefore required with respect to its initial inconsistent performance and requirement for long-term prediction. The model could be improved by justifying the waterfront expansion in the CGP and the base layer contribution.

This pilot site was assessed to have the capability of managing the runoff from 10-year 2-hour rainfall with a 1.4 climate factor from its 120 m^2 catchment. However, the testing site could not be put to use directly as a parking lot, as more refinement is required in terms of the finding balance between surface storage and practical use. Nonetheless, the fundamental mechanism has been revealed by the project, a revelation that will aid the model's future improvement and expansion.

Disclosure statement

This research is an EU project, in cooperation with Klima 2050, Centre for Research-based Innovation (klima2050.no).

Reference

Barry, D. A., J-Y. Parlange, L. Li, D-S. Jeng, and Martin Crapper. 2005. "Green–Ampt approximations." Advances in Water Resources 28 (10): 1003-1009. DOI: 10.1016/j.advwatres.2005.03.010.

Brattebo, Benjamin O., and Derek B. Booth. 2003. "Long-term stormwater quantity and quality performance of permeable pavement systems." Water research 37(18): 4369-4376. DOI:10.1016/S0043-1354(03)00410-X.

Braga, Andrea, Michael Horst, and Robert G. Traver. 2007. "Temperature effects on the infiltration rate through an infiltration basin BMP." Journal of irrigation and drainage engineering 133 (6): 593-601. DOI: 10.1061/(ASCE)0733-9437(2007)133:6(593)

Cao, Su Ling, Daryl Poduska, and Dan G. Zollinger. 1998. *Drainage design and performance guidelines for uni eco-stone permeable pavement*. Uni-Group USA, 1998.

Chow, Ven Te. 2010. *Applied hydrology*. Tata McGraw-Hill Education.

Chu, Shu Tung. 1978 "Infiltration during an unsteady rain." Water Resources Research 14 (3): 461-466. DOI: 10.1029/WR014i003p00461

Collins, Kelly A., William F. Hunt, and Jon M. Hathaway. 2008. "Hydrologic comparison of four types of permeable pavement and standard asphalt in eastern North Carolina." Journal of Hydrologic Engineering 13 (12): 1146-1157. DOI: 10.1061/(ASCE)1084-0699(2008)13:12(1146).

Davis, Allen P. 2008. "Field performance of bioretention: Hydrology impacts." Journal of Hydrologic Engineering 13(2): 90-95. DOI: 10.1061/(ASCE)1084-0699(2008)13:2(90).

Davis, Allen P., Mohammad Shokouhian, Himanshu Sharma, Christie Minami, and Derek Winogradoff. 2003. "Water quality improvement through bioretention: Lead, copper, and zinc removal." Water Environment Research 75(1): 73-82. DOI: 10.2175/106143003X140854.

Dietz, Michael E., and John C. Clausen. 2005. "A field evaluation of rain garden flow and pollutant treatment." Water, Air, and Soil Pollution 167: 123-138. DOI: 10.1007/s11270-005-8266-8.

Dietz, Michael E. 2007. "Low impact development practices: A review of current research and recommendations for future directions." Water, air, and soil pollution no.186: 351-363. DOI 10.1007/s11270-007-9484-z.

Dingman, S. Lawrence. 2015. *Physical hydrology*. Waveland Press.

Facility for Advancing Water Biofiltration (FAWB). 2009. *Stormwater Bioinfiltration Systems. Adorption Guidelines*. Melbourne, Australia.

Guo, James CY, and Ben Urbonas. 2002. "Runoff capture and delivery curves for storm-water quality control designs." Journal of Water Resources Planning and Management 128(3): 208-215. DOI: 10.1061/(ASCE)0733-9496(2002)128:3(208).

Guo, James CY, and Toan M. Luu. 2015. "Hydrologic model developed for stormwater infiltration practices." Journal of Hydrologic Engineering 20(9): 06015001. DOI: 10.1061/(ASCE)HE.1943-5584.0001161

Hanssen-Bauer, Inger, Helge Drange, Eirik J. Førland, Lars A. Roald, Knut Yngve Børsheim, Hege Hisdal, Deborah Lawrence et al. 2009. Klima i Norge 2100. Bakgrunnsmateriale til NOU Klimatilplassing. [Climate in Norway 2100 Background material for NOU Climate adaptation].

Hatt, Belinda E., Tim D. Fletcher, and Ana Deletic. 2009. "Hydrologic and pollutant removal performance of stormwater biofiltration systems at the field scale." Journal of Hydrology 365: 310-321. DOI: 10.1016/j.jhydrol.2008.12.001.

Hunt, W. F., J. T. Smith, S. J. Jadlocki, J. M. Hathaway, and P. R. Eubanks. 2008. "Pollutant removal and peak flow mitigation by a bioretention cell in urban Charlotte, NC." Journal of Environmental Engineering 134(5): 403-408. DOI: 10.1061/(ASCE)0733-9372(2008)134:5(403).

Imran, H. M., Shatirah Akib, and Mohamed Rehan Karim. 2013. "Permeable pavement and stormwater management systems: a review." Environmental technology 34 (18): 2649-2656. DOI: 10.1080/09593330.2013.782573.

James, W., W. R. C James, and H. von Langsdorf. 2013. *Computer aided design of permeable concrete block pavement for reducing stressors and contaminants in an urban environment.* In Proceedings of the seventh international conference on concrete block paving (PAVE AFRICA), Sun City, South Africa. 12-15 October. ISBN: 0-958-46091-4

Johannessen, Birgitte Gisvold, Hans Martin Hanslin, and Tone Merete Muthanna. 2017. "Green roof performance potential in cold and wet regions." Ecological Engineering 106: 436-447. DOI: 10.1016/j.ecoleng.2017.06.011.

Kayhanian, Masoud, Dane Anderson, John T. Harvey, David Jones, and Balasingam Muhunthan. 2012. "Permeability measurement and scan imaging to assess clogging of pervious concrete pavements in parking lots." Journal of Environmental Management 95(1): 114-123. DOI: 10.1016/j.jenvman.2011.09.021.

Kliewer, Dennis Patrick. 2018. "Runoff Modelling and thereon based Dimensioning of Stormwater Management Solutions: Raingarden and Detention Roof by Considering Norwegian Stormwater Management Practices". Master Diss., NTNU & Fachhochschule Münster.

Kuncoro, P. H., K. Koga, N. Satta, and Y. Muto. 2014. "A study on the effect of compaction on transport properties of soil gas and water I: Relative gas diffusivity, air permeability, and saturated hydraulic conductivity." Soil and Tillage Research 143: 172-179. DOI: 10.1016/j.still.2014.02.006.

Li, Houng, Lucas J. Sharkey, William F. Hunt, and Allen P. Davis. 2009. "Mitigation of impervious surface hydrology using bioretention in North Carolina and Maryland." Journal of Hydrologic Engineering 14(4): 407-415. DOI: 10.1061/ASCE1084-0699200914:4407.

Lindholm, Oddvar, Svein Endresen, Sveinn Thorolfsson, Sveinung Sægrov, Guttorm Jakobsen, and Lars Aaby. 2008. Veiledning i klimatilpasset overvannshåndtering [Manual in climate adapted stormwater management]. Norsk vann 162: 8.

McCallum, M. H., J. A. Kirkegaard, T. W. Green, H. P. Cresswell, S. L. Davies, J. F. Angus, and M. B. Peoples. 2004. "Improved subsoil macroporosity following perennial pastures." Australian Journal of Experimental Agriculture 44(3): 299-307. DOI: 10.1071/EA03076

Moghadas, Shahab, A. M. Gustafsson, Peter Viklander, Jiri Marsalek, and Maria Viklander. 2016. "Laboratory study of infiltration into two frozen engineered (sandy) soils recommended for bioretention." Hydrological Processes 30(8): 1251-1264. DOI: 10.1002/hyp.1071

Parnas, Frida Elisif Ågotnes. 2018. "Modelling Runoff from Permeable Surfaces in Urban Areas." Master Diss., NTNU.

Paus, Kim H., Joel Morgan, John S. Gulliver, TorOve Leiknes, and Raymond M. Hozalski. 2014. "Assessment of the hydraulic and toxic metal removal capacities of bioretention cells after 2 to 8 years of service." Water, Air, & Soil Pollution 225(1): 1803. DOI: 10.1007/s11270-013-1803-y

Paus, Kim H., Tone M. Muthanna, and Bent C. Braskerud. 2016. "The hydrological performance of bioretention cells in regions with cold climates: seasonal variation and implications for design." Hydrology Research 47(2): 291-304. DOI: 10.2166/nh.2015.084.

Paus, Kim Aleksander Haukeland. 2016. "Toxic metal removal and hydraulic capacity in bioretention cells in cold climate regions." PhD Diss., NTNU.

Prince George's County. 2009. *The Bioretention manual*. Prince George's County (MD) Government, Department of Environmental Protection.

Rosa, David J., John C. Clausen, and Michael E. Dietz. 2015. "Calibration and validation of SWMM for low impact development." JAWRA Journal of the American Water Resources Association 51(3): 746-757. DOI: 10.1111/jawr.12272.

Rossman, L.A., 2017. *Storm Water Management Model Reference Manual - Volume II - Hydraulics (Manual)*. U.S. Environmental Protection Agency, Cincinnati.

Salvucci, Guido Daniel, and Dara Entekhabi. 1994. "Explicit expressions for Green-Ampt (delta function diffusivity) infiltration rate and cumulative storage." Water Resources Research 30 (9): 2661-2663. DOI: 10.1029/94WR01494

She, Nian, and Joseph Pang. 2009. "Physically based green roof model." Journal of hydrologic engineering 15 (6): 458-464. DOI: 10.1061/(ASCE)HE.1943-5584.0000138.

Statens Vegvesen. 2018. *Håndbok N200 Vegbygging*. https://www.vegvesen.no ISBN: 978-82-7207-723-4

Tollan, Arne. 2002. *Vannressurser*. Universitetsforl.

Trandem, Jens Hissingby. 2016. "Testing of Infiltration System for Stormwater-Permeable Pavement." Master Diss., NTNU.

Weiss, Peter T., Masoud Kayhanian, John S. Gulliver, and Lev Khazanovich. 2019. "Permeable pavement in northern North American urban areas: research review and knowledge gaps." International Journal of Pavement Engineering 20 (2): 143-162. DOI: 10.1080/10298436.2017.1279482.

Whalley, W. R., G. P. Matthews, and Stefano Ferraris. 2012. "The effect of compaction and shear deformation of saturated soil on hydraulic conductivity." Soil and Tillage Research 125: 23-29. DOI: 10.1016/j.still.2012.05.020.

Zhang, Shouhong, and Yiping Guo. 2012. "Explicit equation for estimating storm-water capture efficiency of rain gardens." Journal of Hydrologic Engineering 18(12): 1739-1748. DOI: 10.1061/(ASCE)HE.1943-5584.0000734.

Ødegaard, Hallvard, Sveinung Sægrov, Arve Heistad, Stein Østerhus, Svein Thorolfsson, Gunnar Mosevoll and Oddvar Lindholm. 2012. *Vann- og avløpsteknikk*. Norsk Vann.

Appendices

Appendix 1: Methodology, results and discussion of Alma rain garden

Appendix 2: Experiment

Appendix 3: Calibration result for event 3 and event 4

Appendix 4: Model flow chart

Appendix 5: MATLAB code

Appendix 1: Methodology, results and discussion of Alma rain garden

A1: Hydrologic model

The structure of Alma is presented in Figure A1 left. The effective hydraulic loading i_e has been obtained using equation A1.

$$i_e = P + \frac{Q_{in}}{A} \qquad \text{(A1)}$$

The infiltration mechanism is the same with CGP as described in *3.1.1 Infiltration*, using the explicit GA equation to estimate the potential infiltration rate. As shown in Figure A1 left, part of the growth medium is contained in a concrete basin. Two components, the upper soil and the water reservoir, have therefore been divided without any physical separation. The water stored in the reservoir will remain inside of it except when being absorbed by vegetation, a so-called reservoir for dry conditions. It does not generate many contributions, as it is highly likely to be full when the next rain event starts. Hence, this storage capacity in the reservoir has not been included in the model. It would not be anaerobic due to the presence of the assumed water path, shown in Figure A1 left.

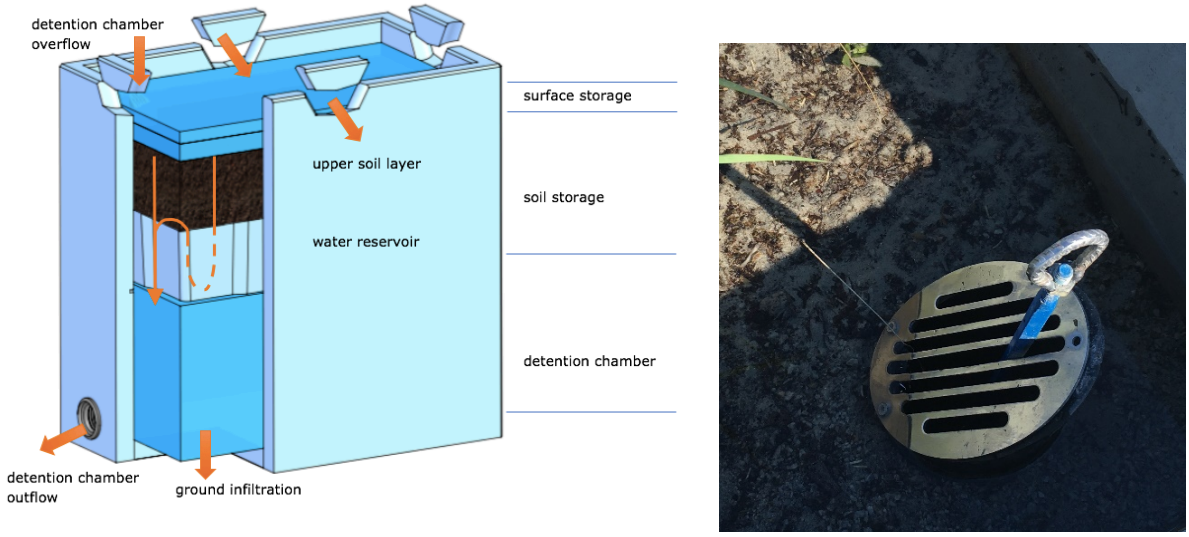

Figure A1: The structure of Alma (left) (Storm Aqua) (Kliewer 2018). The orange lines in the soil layer are the hypothetical flow paths for infiltrated water. The inlet of overflow pipe (right) where the slots have the same width of 8 mm and various lengths of 130, 120, 100 and 60 mm.

Regarding drainage, water in the soil could only leave through the gap and Darcy's Law is therefore not applicable in this situation. The drainage flow has also been assumed to be a proportion of water storage. The contributing area (A_{leak}) and calibration factors γ_1 and γ_2 were obtained from Kliewer (2018) (Equation A2). The drainage flow also determines the actual infiltration rate when the soil is saturated (Equation A3).

$$Q_{leak}(t) = \gamma_1 \left(s(t-1) - s_{fc}\right)^{\gamma_2} \times A_{leak} \qquad \text{(A2)}$$

$$f_a(t) = \begin{cases} min\left(i_e(t) + d(t-1), f_p(t), \Delta s + \frac{Q_{leak}(t)}{H}\right), & \theta < \phi \\ \frac{Q_{leak}(t)}{A}, & \theta = \phi \end{cases} \qquad \text{(A3)}$$

Ponding depth is calculated using equation A4, where $Q_{overflow}$ comprises overflow to the detention chamber and CGP.

$$d(t) = d(t-1) + i_e(t) - f_a(t) - \frac{Q_{overflow}(t)}{A} \quad \text{(A4)}$$

The two overflows were evaluated using level pool routing (LPR) method (Chow 2010) (Equation A5). The storage-discharge (SQ) curve (i.e. $Q \sim \frac{2S}{\Delta t} + Q$) was constructed using discharge equations. As concerns multi-stage outflow, normally a combined SQ curve would be established by accounting for all of the discharge in sequence, leading to a total outflow as the outcome of LPR (NRCS 2004). In order to identify the two spills respectively, the method was modified based on the occurrence order, and the SQ curve was developed for the overflow pipe and weir respectively

$$\frac{2S(t+1)}{\Delta t} + Q(t+1) = \left(I(t+1) + I(t)\right) + \left(\frac{2S(t)}{\Delta t} - Q(t)\right) \quad \text{(A5)}$$

where S is the reservoir storage in the reservoir, I is inflow and Q is outflow.

While the standing pipe functions as the weir or orifice depending on the water level, the transition state has not yet been studied in any depth (Mays, 2001). Only the weir state was considered in the project. Equation A6 was derived from the general weir flow equation to take the unique inlet shape into account (Figure A1 right).

$$Q_{dc} = C_{d1} \int v\, dA = C_{d1} \int \sqrt{2g} h \frac{b\, dh_e}{sin\theta} = \frac{2}{3} C_{d1} \frac{\sqrt{2g} b}{sin\theta} {h_e}^{1.5} \quad \text{(A6)}$$

where b is the slot width, h_e is the effective water level, as $h + 0.001$, θ is the slope of the standing pipe inlet. The coefficient C_{d1} was obtained by calibration.

The trapezoidal weir can be divided into rectangular and V-notch weirs (Subramanya, 1982). Both the contracted rectangular weir (Equation A7) and side weir (Equation A9) exists in Alma. According to a weir definition from Subramanya (1982), they change from broad-crested weir to narrow-crested weir due to the changing $\frac{h}{B}$, where B is the width of crest. It was simplified to apply the broad-crested weir coefficient only (C_{d2}) (Equation A8).

$$Q_r = \frac{2}{3} C_{d2} \sqrt{2g} (L - 0.1nh_e) {h_e}^{1.5} \quad \text{(A7)}$$

$$C_{d2} = 0.521 + 0.028 \frac{h_e}{B} \quad \text{(A8)}$$

As to the rectangular side weirs, the empirical equation used in EPASWMM was chosen, and C_{d4} has been suggested to have a range of 1.5 to 2.6 $ft^{0.5}/s$ (Equation A8, transformed from USC to SI) (Rossman 2017). V-notch weir flow is calculated using equation A9-A11 (Martinez et al. 2005). The total overflow through three trapezoidal weirs has been estimated using equation A12.

$$Q_{sr} = 0{,}301\, C_{d3} \sqrt{2g} (L - 0.1nh_e)^{0.83} {h_e}^{1.67} \quad \text{(A9)}$$

$$Q_t = \frac{8}{15} C_{d4} \sqrt{2g} \tan\frac{\theta}{2} (h + k)^{2.5} \quad \text{(A10)}$$

$$C_{d4} = 0.6072 - 0.000874\theta + 6.1 \times 10^{-6}\theta^2 \quad \text{(A11)}$$

$$k = 4.42 - 0.1035\theta + 1.005 \times 10^{-3}\theta^2 - 3.24 \times 10^{-6}\theta^3 \quad \text{(A12)}$$

$$Q_{tr} = Q_r + 2Q_{sr} + 3Q_t \quad \text{(A13)}$$

In order to perform LPR for each stage, two overflows were prioritized according to their order of occurrence. Consequently, the inflow (I) in equation A5 has to be defined accordingly even though two stages share the same reservoir. The part of water overflow to CGP (Q_C) at (t-1) has been discounted from the inflow for detention chamber overflow (I_D) at t (Equation A14), while the overflow into detention chamber (Q_D) at t had to be withdrawn from the inflow for the CGP overflow (I_C) at t. Moreover, the water level deficit at previous time sequence before the overflow must be deducted (Equation A15).

$$I_D(t) = Q_{in}(t) + P(t)A - \Delta V(t-1) - Q_C(t-1) - Q_d(t) \quad \text{(A14)}$$

$$\Delta V(t-1) = \big(h_D - d(t-1)\big) \times A \quad \text{(A15)}$$

where h_D is the elevation from the surface to the overflow pipe inlet. The obtained discharge from the SQ curve (Q_f) might be higher than the available water volume above the threshold (V_e) and the available space in the detention chamber (V_D). The actual overflow (Q_D) is thereby restrained (Equation 16).

$$Q_D(t) = min\left(Q_f(t),\, V_e(t),\, V_D(t)\right) \quad \text{(A16)}$$

Considering there are two inflows into the detention chamber, it was assumed that the leakage prioritized filling up the detention chamber first (Equation 17).

$$V_D(t) = d_{dc}(t-1) \times A - Q_{leak}(t) \quad \text{(A17)}$$

where d_{dc} is the water level in the detention chamber.

A2: Methodology

The calibration of α' modifying k_{sat} in Alma and C_{d1} was performed based on event 1. The validation was conducted based on event 3.

A sensitivity analysis was conducted to identify the contribution of uncertain parameters using the method stated in 3.4 Sensitivity analysis in order to compensate for the limitations caused by deficient experiments. The analysis was performed based on event 1, while the sensitivity of C_{d2}, C_{d3} and C_{d4} was also estimated using event 3 after considering the fact that they would also affect the accuracy of the CGP model.

A3: Result and Discussion

The NSE of the model after calibration is 0.98 (Figure A2). Event 2 is a complete test involving both Alma and CGP. As previously mentioned, the soil structure was inconsistent in CGP while the Alma result showed efficiency and coherence (Figure 4.3). The biggest discrepancy between the simulated results and observation was at the beginning of the CGP overflow for both events 1 and 2. LPR method requires some time to stabilize, which might be able to improve by using a briefer time sequence. In event 1, there was no interaction between Alma and CGP. The water level stabilized at around 140 mm even though the inflow increased from 60 to 144 l/min, illustrating a sufficient overflow capacity through three weirs. As noted earlier, the main flow path also played a vital role in this process.

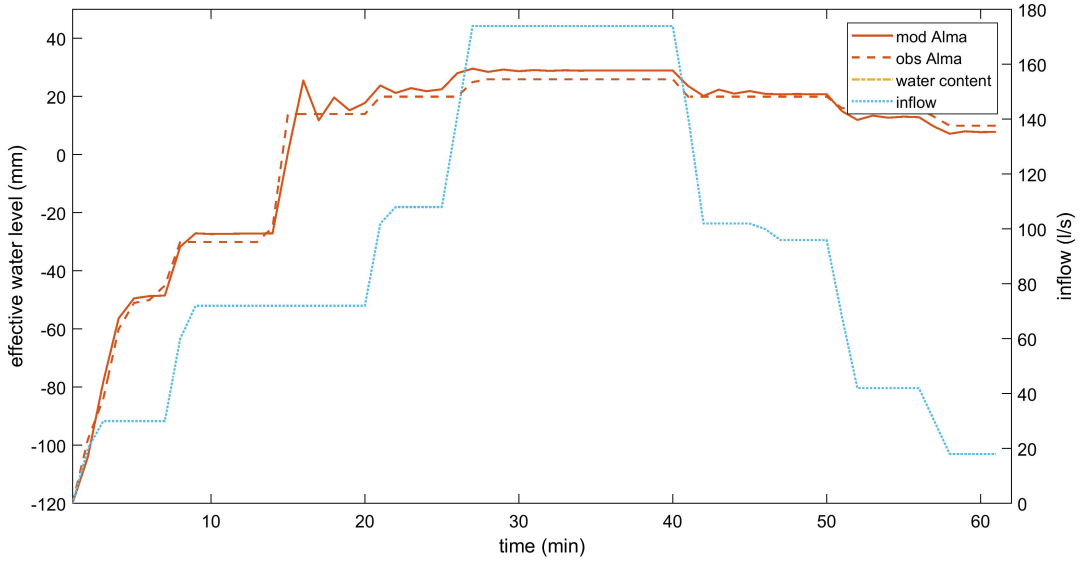

Figure A2: The simulated and observed effective water depth, inflow and water content in Alma based on event 1 (without interaction with CGP) with calibrated factor α'as 0.5.

According to Table A1, C_{d1} was estimated to be the most sensitive parameter, indicating the predominant significance of the model's detention chamber overflow process. Although the subsequent $\Delta\theta$ and γ_2 displayed much less sensitivity, this still shows the influence from the leakage process. If the detention chamber was closed, both the involvement of overflow and leakage would be enhanced as well as the sensitivity of C_{d1}, $\Delta\theta$ and γ_2. The parameters with the lowest sensitivity were ψ_f and α'. The result of the former is coherent and corresponds to its sensitivity results in the CGP model, while the low engagement of k_{sat}.might be attributed to its non-participance in the dominating processes in the Alma model as overflow and leakage.

The sensitivity of CGP overflow coefficients C_d was almost the same in Alma and CGP model (Table A1 and A2). They could to some extent affect the model's accuracy. However, with respect to Alma, the great surface storage in CGP and the main flow path abate the overflow effects on water level, while with respect to CGP, the overflow is mainly controlled by mass balance, and the interaction with LPR only lasts for a short time. If the inflow pattern could be milder and extend the interaction's duration, C_d might play a more vital role. Since the CGP overflow C_d did not experience calibration, their negative sensitivity values manifest the requirement for a further assessment to study the hydraulic characteristics of overflow weir and pipe for the purpose of improving its efficiency level.

The reasons for model imprecision have been discussed, for instance, concern about inflow. Because of confidentiality requirements surrounding Alma, the report's main context was confined to interactive behaviours. The presented Alma model is totally different from the one developed by Kliewer (2018); nonetheless, the model has shown a satisfying symmetry with the observation after applying values for A_{leak}, γ_1 and γ_2 from Kliewer (2018). Hence, the Alma model was actually roughly calibrated and required more work to improve its accuracy. In addition to having a more precise set-up, the water level measurement in the detention chamber would benefit the calibration of leakage and pipe overflow to improve the model's authenticity.

Parameter	+50%	-50%
α'	0.003	0.001
γ_1	-0.003	0.010
γ_2	-0.006	0.038
ψ_f	0.003	0.003
$\Delta\theta$	0.045	-0.006
C_{d1}	0.039	0.235
C_{d2}	-0.005	0.027
C_{d3}	-0.005	0.017
C_{d4}	-0.006	0.020

Table A1: The sensitivity analysis result based on event 1

Parameter	+50%	-50%
C_{d2}	0.017	0.014
C_{d3}	0.002	0.026
C_{d4}	0.014	0.025

Table A2: The sensitivity analysis result based on event 3

Reference

Mays, Larry W. 2001. *Stormwater collection systems design handbook*. McGraw-Hill Professional.

Martinez, J., J. Reca, M. T. Morillas, and J. G. Lopez. 2005. "Design and calibration of a compound sharp-crested weir." Journal of hydraulic Engineering 131(2): 112-116. DOI: 10.1061/(ASCE)0733-9429(2005)131:2(112)

NRCS. 2004. *National Engineering Handbook*: Part 630—Hydrology. USDA Soil Conservation Service: Washington, DC, USA. Chapter 17. https://www.wcc.nrcs.usda.gov/ftpref/wntsc/H&H/NEHhydrology/ch17.pdf

Subramanya, K.1982. *Flow in Open Channels*, 3rd ed. Tata McGraw-Hill Education. Chapter 7

Appendix 2: Experiment

Figure A3: The MPD test, indicating the measurement location and the way it was placed on the surface using silicon. The post-experiment ponding water in Alma was stayed at weir level.

Figure A4: The main flow path noticed during the experiment, also illustrating the hose location, the inflow loss, the slope of curbs and the CGP overflow.

Appendix 3: Calibration result for event 3 and event 4

The total amount of fitting calibration options for event 3 and event 4 with 4 NSEs higher than 0.95 are 4088. Table A3 presents those options giving the best NSE.

	α	ε	β_1	β_2	**NSE3A**	**NSE3C**	**NSE4A**	**NSE4C**
range	0.4-1.0	0.4-0.8	0.6-0.8	0.6-0.8	>0.96	>0.98	>0.97	>0.98
1	0,72	0,56	0,64	0,64	0,965	0,990	0,974	0,984
2	0,72	0,56	0,6	0,68	0,965	0,990	0,974	0,984
3	0,72	0,56	0,62	0,68	0,965	0,985	0,972	0,990
4	0,72	0,56	0,76	0,68	0,965	0,989	0,975	0,984
5	0,72	0,56	0,68	0,72	0,965	0,989	0,973	0,989
6	0,73	0,54	0,72	0,62	0,965	0,989	0,974	0,982
7	0,73	0,54	0,74	0,64	0,965	0,989	0,975	0,984
8	0,73	0,54	0,62	0,66	0,965	0,989	0,973	0,981
9	0,73	0,54	0,66	0,66	0,965	0,989	0,974	0,982
10	0,73	0,54	0,74	0,66	0,965	0,988	0,974	0,982
11	0,73	0,54	0,62	0,74	0,965	0,988	0,974	0,982
12	0,74	0,52	0,66	0,6	0,965	0,983	0,973	0,980
13	0,74	0,52	0,62	0,66	0,965	0,982	0,974	0,981
14	0,75	0,5	0,66	0,66	0,965	0,985	0,974	0,980
15	0,76	0,48	0,74	0,76	0,965	0,981	0,970	0,982
16	0,78	0,44	0,68	0,62	0,966	0,985	0,971	0,990
17	0,78	0,44	0,64	0,74	0,966	0,982	0,972	0,988
18	0,79	0,42	0,7	0,72	0,965	0,980	0,972	0,985

Table A3: A summary of calibration results for event 3 and event 4, where NSE3A and NSE3C are the NSE of Alma and CGP water level respectively the for event 3 and NSE4A and NSE4C are the NSE of Alma and CGP water level respectively the for event 4.

Appendix 4: Model flow chart

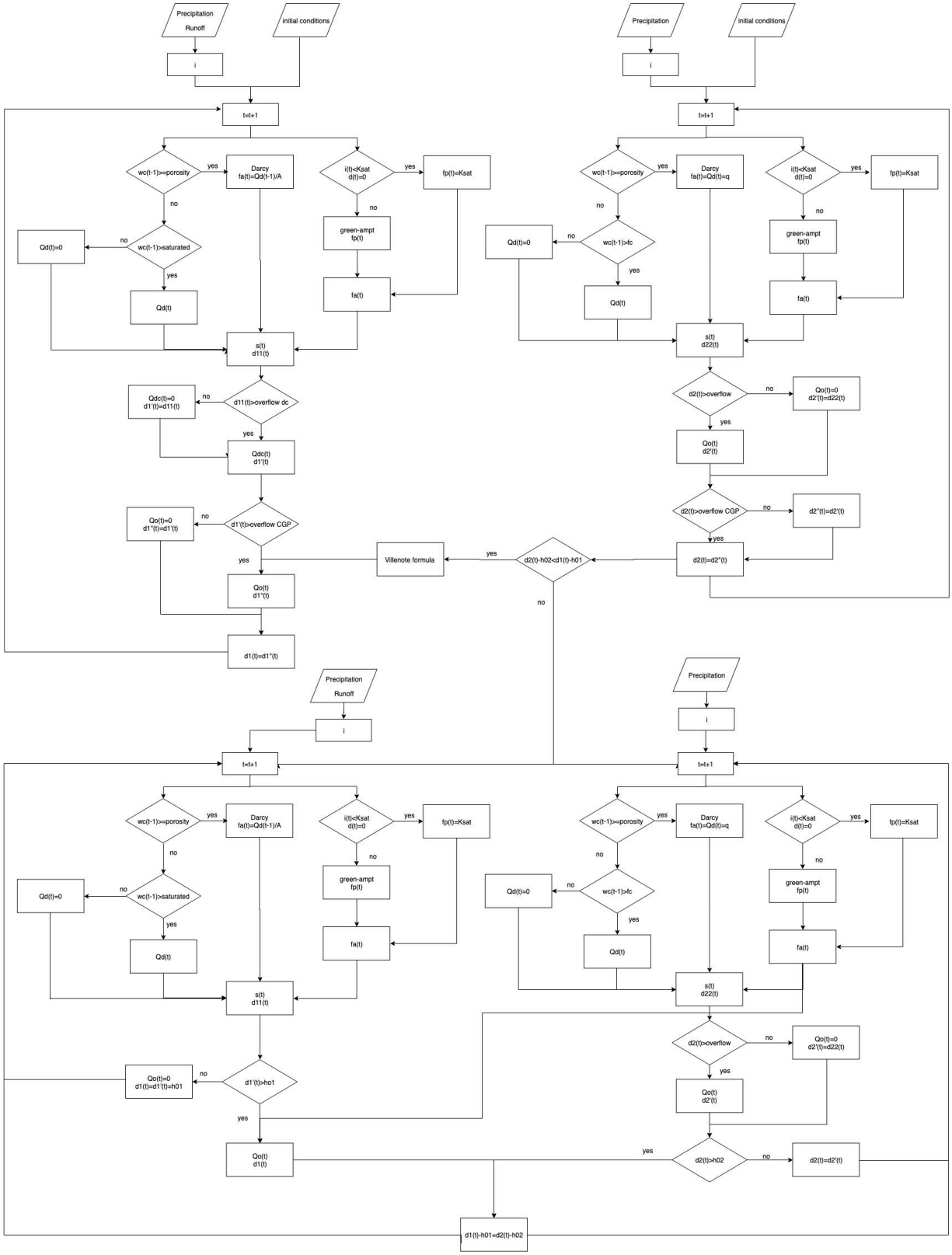

Figure A5: The flow chart of phase 1 and phase 2 in the presented model.

Appendix 5: MATLAB Code

```
%% Input data and preparation
filename = 'input.xlsx';

% event specs
theta_init_A = xlsread(filename,'spec sheet','B14');
theta_init_C = xlsread(filename,'spec sheet','B15');

% site specs
n_alma = xlsread(filename,'spec sheet','B4');
catchmentarea = xlsread(filename,'spec sheet','B7');

%% calibration factor
alpha1=0.9;
alpha2=0.75;
beta1=1.2;                  % leakage from Alma
gamma1 =1.4;
beta2=0.68;                 % unsaturated drainage from CGP
gamma2 =0.80;
epsilon=0.68;               % saturated drainage from CGP for ponding water

%% ALMA RAIN GADEN
width_A=xlsread(filename,'spec sheet','H3');            % width of Alma
length_A=xlsread(filename,'spec sheet','H4');           % length of Alma

% soil properties
veg_A = xlsread(filename,'spec sheet','H12');           % surface vegetation
A_A = xlsread(filename,'spec sheet','H7')*(1-veg_A);
h_soil_A = xlsread(filename,'spec sheet','H8');
ksat_soil_A1 = xlsread(filename,'spec sheet','H9')*alpha1;       % m/s
ksat_soil_A2 = ksat_soil_A1*3600000;                            % mm/h
ksat_soil_A3 = ksat_soil_A1*60000;                              % mm/min
p_soil_A = xlsread(filename,'spec sheet','H10');                % porosity
theta_fc_soil_A = xlsread(filename,'spec sheet','H11');   % field capacity
psi_A = xlsread(filename,'spec sheet','H13');             % suction head
delt_theta_A = p_soil_A - theta_init_A;                   % initial deficit
s_max_A = h_soil_A *p_soil_A;                    % max water content in soil
s_fc_A = h_soil_A *theta_fc_soil_A;

% detention chamber
h_dc = 624+3.14159*(70/1000)^2*0.4*1000/4/A_A;
init_dc_filling = xlsread(filename,'spec sheet','H22');

% overflow to concrete grid pavement
y_full_overflow_A = xlsread(filename,'spec sheet','H33');
h0_overflow_dc = xlsread(filename,'spec sheet','H27');      % from soil surface
to the bottom of overflow pipe
h0_overflow_A = xlsread(filename,'spec sheet','H32');       % from soil surface
to the bottom of spacers
```

```
% Concrete grid pavement
% soil properties
width_C=xlsread(filename,'spec sheet','L4');              % width of CGP
length_C=xlsread(filename,'spec sheet','L5');             % length of CGP
A_C = width_C*length_C-width_A*length_A;
h_C_surf = xlsread(filename,'spec sheet','L7');
void= xlsread(filename,'spec sheet','L8')/100;            % permeable ratio
A_C_soil = A_C*void;

ksat_surf1 = xlsread(filename,'spec sheet','L13')*alpha2;
ksat_surf2 = ksat_surf1*3600000;                          % mm/h
ksat_surf3 = ksat_surf1*60000;                            % mm/min

p_soil_C = xlsread(filename,'spec sheet','L9');           % porosity
theta_fc_soil_C = xlsread(filename,'spec sheet','L12');   % field capacity
theta_max_soil_C = p_soil_C;                            % max water content
psi_C = xlsread(filename,'spec sheet','L14');           % mm suction head
veg_C = xlsread(filename,'spec sheet','L11');           % surface vegetation

delt_theta_C = p_soil_C - theta_init_C;
s_max_C = h_C_surf *p_soil_C;

% structure of concrete grid pavement
h_C_spacer = xlsread(filename,'spec sheet','L17');        % to spacers
y_full_overflow_f = xlsread(filename,'spec sheet','L22');
h0_overflow_f = xlsread(filename,'spec sheet','L21');     % to outflow weir


% input for Level pool routing
x1=xlsread(filename,'orrifice - weir specs','H4:H65536');
x1=x1(:);
y1=xlsread(filename,'orrifice - weir specs','F4:F65536');
y1=y1(:);                                  % overflow into detention chamber

theta=112;
Cd=0.6072-0.000874*112+6.1*10^(-6)*112^2;
k=4.42-0.1035*112+1*10^(-3)*112^2-3.24*10^(-6)*112^3;
for t=1:94
    h(t)=t;
    Lw(t)=(150-0.2*h(t))/1000;
    Qt1(t)=2/3*(2*9.8)^0.5*Lw(t)*60000*(h(t)/1000)^1.5*(0.028*h(t)/80+0.521);
    Qt2(t)=2*(Lw(t)/0.3048)^0.83*(h(t)/0.3048)^1.67*1.5*0.55*0.0283168;

Qr(t)=(8/15)*Cd*(2*9.81)^0.5*tan(theta*pi/360)*((h(t)+k)/1000)^(5/2)*(1000*60)
;
    y2(t)=(Qt1(t)+Qt2(t)+Qr(t)*3);
    s2(t)=h(t)*0.941;
    x2(t)=2*s2(t)+y2(t);                   % overflow to CGP
```

```
    s3(t)=(9.245+19.85*t/1000+9.47*t^2/1000000-0.88*1.48+A_C)*t/2;
    y3(t)= Qt1(t);
    x3(t)=2*s3(t)+y3(t);                    % final overflow
end


%% initial state
d11(1)=0;
d1(1)=0;                                    % ponding water depth
Q_leak(1)=0;                                % leakage from Alma
fact(1) =0;                                 % actualu infiltration rate
fpot(1)=ksat_soil_A3;                       % potential infiltraiton rate
s_soil(1)=theta_init_A*h_soil_A;            % initial water content, mm
theta_soil(1)=theta_init_A;                 % initial water content
d_dc(1)=init_dc_filling*h_dc;               % initial water level in chamber

% overflow to detention chamber
he_overflow(1)=0;
ie_overflow(1)=0;
I_DC(1)=0;                                  % I(t)+I(t+1)
SQ_DC(1)=0;                                 % 2S(t)-Q(t)
sq_DC(1)=0;                                 % 2S(t+1)+Q(t+1)
Q_dc_in(1)=0;

% overflow to concrete grid pavement
he_overflowinC(1)=0;
ie_overflowinC(1)=0;
I_C(1)=0;
SQ_C(1)=0;
sq_C(1)=0;
Q_C_in(1)=0;

% Concrete grid pavement - surface
i_C(1)=0;
fpot_C(1) =ksat_surf3;
fact_C(1) =0;
s_soil_C(1) =theta_init_C*h_C_surf;
theta_soil_C(1) =theta_init_C;
d2(1) =0;
d22(1)=0;
Qd(1)=0;

% Final overflow from concrete grid pavement
he_overflow_f(1) =0;
ie_overflow_f(1) =0;
I_f(1) =0;
SQ_f(1) =0;
Q_f_overflow(1) =0;
sq_f(1) =0;
```

```
% GA for Alma
f_m(1)=0;
tp1(1)=0;
tc1(1)=0;
C1(1)=0;

% GA for CGP
f_m2(1)=0;
tp2(1)=0;
tc2(1)=0;
C2(1)=0;

%% Calculation
% Runoff/inflow into Alma
prec=xlsread(filename,'prec','D3:D123');
Q=prec*catchmentarea;                                          % L/min
i_e=prec+Q/A_A;
duration = length(prec);

breakpoint=0;

for t=2:duration

    [f_m(t),C1(t),tc1(t),tp1(t),  T1(t),FP1(t),te1(t)]  =  GA(t,  C1(t-1),  i_e,
ksat_soil_A2, ksat_soil_A3, psi_A, d11(t-1), delt_theta_A, tp1(t-1), tc1(t-1),
fact, Q_leak);

    % potential infiltration rate
    if i_e(t)<ksat_soil_A3 && d11(t-1)<=0
        fpot(t) = ksat_soil_A3;
    else
        fpot(t) = f_m(t);
    end

    % actual infiltration rate
    if theta_soil(t-1)>=p_soil_A
        fact(t)=Q_leak(t-1)/A_A;
    else     fact(t)=min([fpot(t),i_e(t)+d11(t-1),s_max_A-s_soil(t-1)+Q_leak(t-
1)/A_A]);
    end

    s_soil(t)=min(s_soil(t-1)+fact(t)-Q_leak(t-1)/A_A,s_max_A);
    theta_soil(t) = s_soil(t)/h_soil_A;

    % Q_leak(t)
    CLA=A_A*0.1;
    if theta_soil(t)>theta_fc_soil_A
        Q1(t)=beta1*CLA*(s_soil(t)-s_fc_A)^gamma1;
    else
        Q1(t)=0;
```

```
    end

    if d_dc(t-1)<h_dc
        Q_leak(t)=min(Q1(t),(h_dc-d_dc(t-1))*A_A);
    else
        Q_leak(t)= 0;
    end

    % ponding water level
    d11(t)=d1(t-1)+i_e(t)-fact(t);

    % Alma overflow to detention chamber
    [ Q_dc_i(t), ie_overflow(t),sq_DC(t), he_overflow(t)] = ALMAOVERFLOW( x1,
y1, d11(t), h0_overflow_dc, he_overflow(t-1), ie_overflow(t-1),sq_DC(t-1), A_A,
i_e(t), fact(t),Q_C_in(t-1) );

    if he_overflow(t)>0
        if d_dc(t-1)<h_dc
            Q_dc_in(t)=min(min(Q_dc_i(t),(h_dc-d_dc(t-1))*A_A-
Q_leak(t)),he_overflow(t)*A_A);
        else
            Q_dc_in(t)= 0;
        end
    else
        Q_dc_in(t)= 0;
    end

    % water level in detention chamber
    d_dc(t)=min(h_dc,(Q_dc_in(t)+Q_leak(t))/A_A+d_dc(t-1));

    % overflow to concrete grid pavement
    he_overflowinC(t)=d11(t)-Q_dc_in(t)/A_A-h0_overflow_A;

    if he_overflowinC(t)<=0
        ie_overflowinC(t)= 0;
    elseif he_overflowinC(t-1)<=0
        ie_overflowinC(t)=    max(0,(i_e(t)-fact(t)+he_overflowinC(t-1))*A_A)-
Q_dc_in(t);
    else ie_overflowinC(t)= max(0,(i_e(t)-fact(t))*A_A)-Q_dc_in(t);
    end

    I_C(t)= ie_overflowinC(t-1)+ ie_overflowinC(t);
    SQ_C(t)=I_C(t)+sq_C(t-1);

    if he_overflowinC(t)>0
        if d2(t-1)-h_C_spacer <=0
            Q_C_i(t)=interp1(x2,y2,SQ_C(t),'pchip');
            Q_C_in(t)=min(he_overflowinC(t)*A_A, Q_C_i(t));
        else
            y21=y2*(1-((d2(t-1)-h_C_spacer)/he_overflowinC(t))^1.5)^0.385;
```

```
            x21=2*s2+y21;
            Q_C_i(t)=interp1(x21,y21,SQ_C(t),'pchip');
            Q_C_in(t)=min(he_overflowinC(t)*A_A, Q_C_i(t));                    %
modify the S-Q curve according to each d1 and d2
        end
    else
        Q_C_in(t)=0;
    end

    sq_C(t)= SQ_C(t)-2*Q_C_in(t);

    if d2(t-1)<=0
        if prec(t)/void+Q_C_in(t)/A_C_soil <=ksat_surf3 && s_max_C-s_soil_C(t-
1)>=ksat_surf3
            i_C(t)=prec(t)/void+Q_C_in(t)/A_C_soil;
        else
            i_C(t)=prec(t)+Q_C_in(t)/A_C;
        end
    else
        i_C(t)=prec(t)+Q_C_in(t)/AREA(d2(t-1));
    end

    [f_m2(t),C2(t),tc2(t),tp2(t),T2(t),te2(t)]    =    GA(t,    C2(t-1),    i_C,
ksat_surf2,  ksat_surf3,  psi_C,  d2(t-1),  delt_theta_C,  tp2(t-1),  tc2(t-1),
fact_C, Qd);


    % potential infiltration rate
    if i_C(t)<ksat_surf3 && d2(t-1)<=0
        fpot_C(t) = ksat_surf3;
    else
        fpot_C(t) = f_m2(t);
    end

    % Q_d drainage
    if theta_soil_C(t-1)>=theta_fc_soil_C
        if theta_soil_C(t-1)< p_soil_C
            Qd(t)=beta2*(s_soil_C(t-1)-
theta_fc_soil_C*h_C_surf)^gamma2*A_C_soil;
        else Qd(t)=ksat_surf3*(1+d2(t-1)*epsilon/h_C_surf)*A_C_soil;
        end
    else
        Qd(t)=0;
    end

    ppS(t)=s_max_C-s_soil_C(t-1)+Qd(t)/A_C_soil;       % available soil storage
    if d2(t-1)>0
        ppH(t)=(i_C(t)+d2(t-1))/void*0.8;
    else
        ppH(t)=i_C(t);                                 % available standing water
```

```
    end

    if theta_soil_C(t-1)>=p_soil_C
        fact_C(t)=min(ksat_surf3*(1+d2(t-1)*epsilon/h_C_surf),ppH(t));
    else
        fact_C(t)=min(min(fpot_C(t),ppH(t)),ppS(t));
    end

    s_soil_C(t)=min(s_soil_C(t-1)+fact_C(t)-Qd(t)/A_C_soil,s_max_C);
    theta_soil_C(t) = s_soil_C(t)/h_C_surf;

    % ponding water level
    if d2(t-1)<=0
        d22(t)= d2(t-1)+i_C(t)-fact_C(t);
    else
        d22(t)= d2(t-1)+prec(t)+(Q_C_in(t)-fact_C(t)*A_C_soil)/AREA(d2(t-1));
    end

    [   Q_f_overflow(t),   ie_overflow_f(t),sq_f(t),   he_overflow_f(t)]   =
CGPOVERFLOW(   x3,   y3,   d22(t),   h0_overflow_f,   he_overflow_f(t-1),
ie_overflow_f(t-1),sq_f(t-1), Q_C_in(t) );

    d2(t)=d22(t)-Q_f_overflow(t)/AREA(d22(t));
    d1(t)=d11(t)-Q_C_in(t)/A_A-Q_dc_in(t)/A_A;

    if d2(t)-h_C_spacer>d1(t)-h0_overflow_A && d1(t)-h0_overflow_A>0
        breakpoint=t;
        break
    end
end

if breakpoint==0
    for t=duration+1:500
        Q(t)=0;
        i_e(t)=0;

        [f_m(t),C1(t),tc1(t),tp1(t), T1(t),FP1(t),te1(t)] = GA(t, C1(t-1), i_e,
ksat_soil_A2, ksat_soil_A3, psi_A, d11(t-1), delt_theta_A, tp1(t-1), tc1(t-1),
fact, Q_leak);

        % potential infiltration rate
        if i_e(t)<ksat_soil_A3 && d11(t-1)<=0
            fpot(t) = ksat_soil_A3;
        else
            fpot(t) = f_m(t);
        end

        % actual infiltration rate
        if theta_soil(t-1)>=p_soil_A
            fact(t)=Q_leak(t-1)/A_A;
```

```
        else            fact(t)=min([fpot(t),i_e(t)+d11(t-1),s_max_A-s_soil(t-
1)+Q_leak(t-1)/A_A]);
        end

        s_soil(t)=min(s_soil(t-1)+fact(t)-Q_leak(t-1)/A_A,s_max_A);
        theta_soil(t) = s_soil(t)/h_soil_A;

        % Q_leak(t)
        CLA=A_A*0.1;
        if theta_soil(t)>theta_fc_soil_A
            Q1(t)=beta1*CLA*(s_soil(t)-s_fc_A)^gamma1;
        else
            Q1(t)=0;
        end

        if d_dc(t-1)<h_dc
            Q_leak(t)=min(Q1(t),(h_dc-d_dc(t-1))*A_A);
        else
            Q_leak(t)= 0;
        end

        % ponding water level
        d11(t)=d1(t-1)+i_e(t)-fact(t);

        % Alma overflow to detention chamber
        [ Q_dc_i(t), ie_overflow(t),sq_DC(t), he_overflow(t)] = ALMAOVERFLOW(
x1, y1, d11(t), h0_overflow_dc, he_overflow(t-1), ie_overflow(t-1),sq_DC(t-1),
A_A, i_e(t), fact(t),Q_C_in(t-1) );

        if he_overflow(t)>0
            if d_dc(t-1)<h_dc
                Q_dc_in(t)=min(min(Q_dc_i(t),(h_dc-d_dc(t-1))*A_A-
Q_leak(t)),he_overflow(t)*A_A);
            else
                Q_dc_in(t)= 0;
            end
        else
            Q_dc_in(t)= 0;
        end

        % water level in detention chamber
        d_dc(t)=min(h_dc,(Q_dc_in(t)+Q_leak(t))/A_A+d_dc(t-1));

        % overflow to concrete grid pavement
        he_overflowinC(t)=d11(t)-Q_dc_in(t)/A_A-h0_overflow_A;

        if he_overflowinC(t)<=0
            ie_overflowinC(t)= 0;
        elseif he_overflowinC(t-1)<=0
```

```
            ie_overflowinC(t)=          max(0,(i_e(t)-fact(t)+he_overflowinC(t-
1))*A_A)-Q_dc_in(t);
        else ie_overflowinC(t)= max(0,(i_e(t)-fact(t))*A_A)-Q_dc_in(t);
        end

        I_C(t)= ie_overflowinC(t-1)+ ie_overflowinC(t);
        SQ_C(t)=I_C(t)+sq_C(t-1);

        if he_overflowinC(t)>0
            if d2(t-1)-h_C_spacer <=0
                Q_C_i(t)=interp1(x2,y2,SQ_C(t),'pchip');
                Q_C_in(t)=min(he_overflowinC(t)*A_A, Q_C_i(t));
            else
                y21=y2*(1-((d2(t-1)-h_C_spacer)/he_overflowinC(t))^1.5)^0.385;
                x21=2*s2+y21;
                Q_C_i(t)=interp1(x21,y21,SQ_C(t),'pchip');
                Q_C_in(t)=min(he_overflowinC(t)*A_A, Q_C_i(t));              %
modify the S-Q curve according to each d1 and d2
            end
        else
            Q_C_in(t)=0;
        end

        sq_C(t)= SQ_C(t)-2*Q_C_in(t);

        i_C(t)=prec(t)+Q_C_in(t)/AREA(d2(t-1));

        [f_m2(t),C2(t),tc2(t),tp2(t),T2(t),te2(t)]   =   GA(t,   C2(t-1),   i_C,
ksat_surf2,  ksat_surf3,  psi_C,  d2(t-1),  delt_theta_C,  tp2(t-1),  tc2(t-1),
fact_C, Qd);


        % potential infiltration rate
        if i_C(t)<ksat_surf3 && d2(t-1)<=0
            fpot_C(t) = ksat_surf3;
        else
            fpot_C(t) = f_m2(t);
        end

        % Q_d drainage
        if theta_soil_C(t-1)>=theta_fc_soil_C
            if theta_soil_C(t-1)< p_soil_C-0.02
                Qd(t)=beta2*(s_soil_C(t-1)-
theta_fc_soil_C*h_C_surf)^gamma2*A_C_soil;
            else Qd(t)=ksat_surf3*(1+d2(t-1)*epsilon/h_C_surf)*A_C_soil;
            end
        else
            Qd(t)=0;
        end
```

```
        ppS(t)=s_max_C-s_soil_C(t-1)+Qd(t)/A_C_soil;    % available soil storage

        if d2(t-1)>0
            ppH(t)=(i_C(t)+d2(t-1))/void*0.8;
        else
            ppH(t)=i_C(t);                              % available standing water
        end

        if theta_soil_C(t-1)>=p_soil_C-0.02
            fact_C(t)=min(ksat_surf3*(1+d2(t-1)*epsilon/h_C_surf),ppH(t));
        else
            fact_C(t)=min(min(fpot_C(t),ppH(t)),ppS(t));
        end

        s_soil_C(t)=min(s_soil_C(t-1)+fact_C(t)-Qd(t)/A_C_soil,s_max_C);
        theta_soil_C(t) = s_soil_C(t)/h_C_surf;

        % ponding water level
        if d2(t-1)<=0
            d22(t)= d2(t-1)+i_C(t)-fact_C(t);
        else
            d22(t)=   d2(t-1)+prec(t)+(Q_C_in(t)-fact_C(t)*A_C_soil)/AREA(d2(t-
1));
        end

        [   Q_f_overflow(t),   ie_overflow_f(t),sq_f(t),   he_overflow_f(t)]   =
CGPOVERFLOW(    x3,    y3,    d22(t),    h0_overflow_f,    he_overflow_f(t-1),
ie_overflow_f(t-1),sq_f(t-1), Q_C_in(t) );

        d2(t)=d22(t)-Q_f_overflow(t)/AREA(d22(t));
        d1(t)=d11(t)-Q_C_in(t)/A_A-Q_dc_in(t)/A_A;

        if d2(t)<1
            break
        end

    end
else

    for t=breakpoint:500
        if t>duration
            Q(t)=0;
            i_e(t)=0;
            prec(t)=0;
        end

        % GA infiltraiton in Alma
        [f_m(t),C1(t),tc1(t),tp1(t), T1(t),FP1(t),te1(t)] = GA(t, C1(t-1), i_e,
ksat_soil_A2, ksat_soil_A3, psi_A, d11(t-1), delt_theta_A, tp1(t-1), tc1(t-1),
fact, Q_leak);
```

```
        % potential infiltration rate
        if i_e(t)<ksat_soil_A3 && d11(t-1)<=0
            fpot(t) = ksat_soil_A3;
        else
            fpot(t) = f_m(t);
        end

        % actual infiltration rate
        if theta_soil(t-1)>=p_soil_A
            fact(t)=Q_leak(t-1)/A_A;
        else            fact(t)=min([fpot(t),i_e(t)+d11(t-1),s_max_A-s_soil(t-
1)+Q_leak(t-1)/A_A]);
        end

        s_soil(t)=min(s_soil(t-1)+fact(t)-Q_leak(t-1)/A_A,s_max_A);
        theta_soil(t) = s_soil(t)/h_soil_A;

        % Q_leak(t)
        CLA=A_A*0.1;
        if theta_soil(t)>theta_fc_soil_A
            Q1(t)=beta1*CLA*(s_soil(t)-s_fc_A)^gamma1;
        else
            Q1(t)=0;
        end

        if d_dc(t-1)<h_dc
            Q_leak(t)=min(Q1(t),(h_dc-d_dc(t-1))*A_A);
        else
            Q_leak(t)= 0;
        end

        % ponding water level
        d11(t)=d1(t-1)+i_e(t)-fact(t);

        % Alma overflow to detention chamber
        [ Q_dc_i(t), ie_overflow(t), sq_DC(t), he_overflow(t)] = ALMAOVERFLOW(
x1, y1, d11(t), h0_overflow_dc, he_overflow(t-1), ie_overflow(t-1),sq_DC(t-1),
A_A, i_e(t), fact(t),Q_C_in(t-1) );

        if d_dc(t-1)<h_dc
            Q_dc_in(t)=min(Q_dc_i(t),(h_dc-d_dc(t-1))*A_A-
Q_leak(t),he_overflow(t)*A_A);
        else
            Q_dc_in(t)= 0;
        end

        % Alma detention chamber
        d_dc(t)=min(h_dc,(Q_dc_in(t)+Q_leak(t))/A_A+d_dc(t-1));
```

```
        % Alma overflow to concrete grid pavement
        he_overflowinC(t)=d11(t)-Q_dc_in(t)/A_A-h0_overflow_A;
        i_C(t)=prec(t)+Q(t)/(AREA(d2(t-1))+0.88*1.48);

        % GA infiltration rate in CGP
        [f_m2(t),C2(t),tc2(t),tp2(t),T2(t),TP2(t),te2(t)] = GA(t, C2(t-1), i_C,
ksat_surf2,  ksat_surf3,  psi_C,  d2(t-1),  delt_theta_C,  tp2(t-1),  tc2(t-1),
fact_C, Qd);

        % potential infiltration rate
        if i_C(t)<ksat_surf3 && d2(t-1)<=0
            fpot_C(t) = ksat_surf3;
        else
            fpot_C(t) = f_m2(t);
        end

        % Qd drainage
        if theta_soil_C(t-1)< p_soil_C-0.02
            if theta_soil_C(t-1)>=theta_fc_soil_C
                Qd(t)=beta2*(s_soil_C(t-1)
theta_fc_soil_C*h_C_surf)^gamma2*A_C_soil;
            else
                Qd(t)=0;
            end
        else
            Qd(t)=ksat_surf3*(1+d2(t-1)*epsilon/h_C_surf)*A_C_soil;
        end

        ppS(t)=s_max_C-s_soil_C(t-1)+Qd(t)/A_C_soil;    % available soil storage
        if d2(t-1)>0
            ppH(t)=(i_C(t)+d2(t-1))/void*0.8;
        else
            ppH(t)=i_C(t)+d2(t-1);                    % available standing water
        end

        if theta_soil_C(t-1)>=p_soil_C-0.02
            fact_C(t)=min(ksat_surf3*(1+d2(t-1)*epsilon/h_C_surf),ppH(t));
        else
            fact_C(t)=min(min(fpot_C(t),ppH(t)),ppS(t));
        end

        [   Q_f_overflow(t),   ie_overflow_f(t),sq_f(t),   he_overflow_f(t)]   =
CGPOVERFLOW(    x3,    y3,    d2(t-1),    h0_overflow_f,    he_overflow_f(t-1),
ie_overflow_f(t-1),sq_f(t-1), Q_C_in(t-1));

        if he_overflowinC(t)>0
            delta_level(t)=(Q(t)-fact_C(t)*A_C_soil-
Q_f_overflow(t))/(AREA(d2(t-1))+A_A);
            Q_C_i(t)=Q(t)-delta_level(t)*A_A;
```

```
            Q_C_in(t)=min(he_overflowinC(t)*A_A, Q_C_i(t));
        else
            Q_C_in(t)=0;
        end

        he_overflowinC(t)=d11(t)-Q_dc_in(t)/A_A-h0_overflow_A;

        if he_overflowinC(t)<=0
            ie_overflowinC(t)= 0;
        elseif he_overflowinC(t-1)<=0
            ie_overflowinC(t)=          max(0,(i_e(t)-fact(t)+he_overflowinC(t-
1))*A_A)-Q_dc_in(t);
        else ie_overflowinC(t)= max(0,(i_e(t)-fact(t))*A_A)-Q_dc_in(t);
        end

        I_C(t)= ie_overflowinC(t-1)+ ie_overflowinC(t);
        SQ_C(t)=I_C(t)+sq_C(t-1);
        sq_C(t)= SQ_C(t)-2*Q_C_in(t);

        s_soil_C(t)=min(s_soil_C(t-1)+fact_C(t)-Qd(t)/A_C_soil,s_max_C);
        theta_soil_C(t) = s_soil_C(t)/h_C_surf;

        % ponding water level in CGP
        if d2(t-1)<=0
            d2(t)= d2(t-1)+prec(t)+Q_C_in(t)/A_C_soil-fact_C(t);
        else
            d2(t)=               d2(t-1)+prec(t)+(Q_C_in(t)-fact_C(t)*A_C_soil-
Q_f_overflow(t))/AREA(d2(t-1));
        end

        d1(t)=d11(t)-Q_C_in(t)/A_A-Q_dc_in(t)/A_A;

        if d1(t)-h0_overflow_A==0
            if t<duration
                break
            end

            if d2(t)<1
                break
            end

        end
    end
end

restratponit=t;

if restratponit<=duration
    for t=restratponit+1:500
        if t>duration
```

```
            Q(t)=0;
            i_e(t)=0;
            prec(t)=0;
        end

        [f_m(t),C1(t),tc1(t),tp1(t), T1(t),FP1(t),te1(t)] = GA(t, C1(t-1), i_e,
ksat_soil_A2, ksat_soil_A3, psi_A, d11(t-1), delt_theta_A, tp1(t-1), tc1(t-1),
fact, Q_leak);

        % potential infiltration rate
        if i_e(t)<ksat_soil_A3 && d11(t-1)<=0
            fpot(t) = ksat_soil_A3;
        else
            fpot(t) = f_m(t);
        end

        % actual infiltration rate
        if theta_soil(t-1)>=p_soil_A
            fact(t)=Q_leak(t-1)/A_A;
        else            fact(t)=min([fpot(t),i_e(t)+d11(t-1),s_max_A-s_soil(t-
1)+Q_leak(t-1)/A_A]);
        end

        s_soil(t)=min(s_soil(t-1)+fact(t)-Q_leak(t-1)/A_A,s_max_A);
        theta_soil(t) = s_soil(t)/h_soil_A;

        % Q_leak(t)
        CLA=A_A*0.1;                                          % leakage area
        if theta_soil(t)>theta_fc_soil_A
            Q1(t)=beta1*CLA*(s_soil(t)-s_fc_A)^gamma1;
        else
            Q1(t)=0;
        end

        if d_dc(t-1)<h_dc
            Q_leak(t)=min(Q1(t),(h_dc-d_dc(t-1))*A_A);
        else
            Q_leak(t)= 0;
        end

        % ponding water level
        d11(t)=d1(t-1)+i_e(t)-fact(t);

        % Alma overflow to detention chamber
        [ Q_dc_i(t), ie_overflow(t),sq_DC(t), he_overflow(t)] = ALMAOVERFLOW(
x1, y1, d11(t), h0_overflow_dc, he_overflow(t-1), ie_overflow(t-1),sq_DC(t-1),
A_A, i_e(t), fact(t),Q_C_in(t-1) );

        if he_overflow(t)>0
            if d_dc(t-1)<h_dc
```

```
                Q_dc_in(t)=min(min(Q_dc_i(t),(h_dc-d_dc(t-1))*A_A-
Q_leak(t)),he_overflow(t)*A_A);
            else
                Q_dc_in(t)= 0;
            end
        else
            Q_dc_in(t)= 0;
        end

        % water level in detention chamber
        d_dc(t)=min(h_dc,(Q_dc_in(t)+Q_leak(t))/A_A+d_dc(t-1));

        % overflow to concrete grid pavement
        he_overflowinC(t)=d11(t)-Q_dc_in(t)/A_A-h0_overflow_A;

        if he_overflowinC(t)<=0
            ie_overflowinC(t)= 0;
        elseif he_overflowinC(t-1)<=0
            ie_overflowinC(t)=          max(0,(i_e(t)-fact(t)+he_overflowinC(t-
1))*A_A)-Q_dc_in(t);
        else ie_overflowinC(t)= max(0,(i_e(t)-fact(t))*A_A)-Q_dc_in(t);
        end

        I_C(t)= ie_overflowinC(t-1)+ ie_overflowinC(t);
        SQ_C(t)=I_C(t)+sq_C(t-1);

        if he_overflowinC(t)>0
            if d2(t-1)-h_C_spacer <=0
                Q_C_i(t)=interp1(x2,y2,SQ_C(t),'pchip');
                Q_C_in(t)=min(he_overflowinC(t)*A_A, Q_C_i(t));
            else
                y21=y2*(1-((d2(t-1)-h_C_spacer)/he_overflowinC(t))^1.5)^0.385;
                x21=2*s2+y21;
                Q_C_i(t)=interp1(x21,y21,SQ_C(t),'pchip');
                Q_C_in(t)=min(he_overflowinC(t)*A_A, Q_C_i(t));                %
modify the S-Q curve according to each d1 and d2
            end
        else
            Q_C_in(t)=0;
        end

        sq_C(t)= SQ_C(t)-2*Q_C_in(t);

        if d2(t-1)<=0
            if   prec(t)/void+Q_C_in(t)/A_C_soil   <=ksat_surf3   &&   s_max_C-
s_soil_C(t-1)>=ksat_surf3
                i_C(t)=prec(t)/void+Q_C_in(t)/A_C_soil;                    else
                i_C(t)=prec(t)+Q_C_in(t)/A_C;
            end
        else
```

```
            i_C(t)=prec(t)+Q_C_in(t)/AREA(d2(t-1));
        end

        [f_m2(t),C2(t),tc2(t),tp2(t),T2(t),te2(t)]   =   GA(t,   C2(t-1),   i_C,
ksat_surf2,  ksat_surf3,  psi_C,  d2(t-1),  delt_theta_C,  tp2(t-1),  tc2(t-1),
fact_C, Qd);


        % potential infiltration rate
        if i_C(t)<ksat_surf3 && d2(t-1)<=0
            fpot_C(t) = ksat_surf3;
        else
            fpot_C(t) = f_m2(t);
        end

        % Q_d drainage
        if theta_soil_C(t-1)>=theta_fc_soil_C
            if theta_soil_C(t-1)< p_soil_C
                Qd(t)=beta2*(s_soil_C(t-1)-
theta_fc_soil_C*h_C_surf)^gamma2*A_C_soil;
            else Qd(t)=ksat_surf3*(1+d2(t-1)*epsilon/h_C_surf)*A_C_soil;
            end
        else
            Qd(t)=0;
        end

        ppS(t)=s_max_C-s_soil_C(t-1)+Qd(t)/A_C_soil;    % available soil storage

        if d2(t-1)>0
            ppH(t)=(i_C(t)+d2(t-1))/void*0.8;
        else
            ppH(t)=i_C(t);                              % available standing water
        end

        if theta_soil_C(t-1)>=p_soil_C
            fact_C(t)=min(ksat_surf3*(1+d2(t-1)*epsilon/h_C_surf),ppH(t));
        else
            fact_C(t)=min(min(fpot_C(t),ppH(t)),ppS(t));
        end

        s_soil_C(t)=min(s_soil_C(t-1)+fact_C(t)-Qd(t)/A_C_soil,s_max_C);
        theta_soil_C(t) = s_soil_C(t)/h_C_surf;

        % ponding water level
        if d2(t-1)<=0
            d22(t)= d2(t-1)+i_C(t)-fact_C(t);
        else
            d22(t)=   d2(t-1)+prec(t)+(Q_C_in(t)-fact_C(t)*A_C_soil)/AREA(d2(t-
1));
        end
```

```
        [   Q_f_overflow(t),   ie_overflow_f(t),sq_f(t),   he_overflow_f(t)]   =
CGPOVERFLOW(    x3,    y3,    d22(t),    h0_overflow_f,    he_overflow_f(t-1),
ie_overflow_f(t-1),sq_f(t-1), Q_C_in(t) );

        d2(t)=d22(t)-Q_f_overflow(t)/AREA(d22(t));
        d1(t)=d11(t)-Q_C_in(t)/A_A-Q_dc_in(t)/A_A;

        if d2(t)<1 && d1(t)-h0_overflow_A <1
            break
        end

    end
end


function [ A ] = AREA( pond)
% varying area in the CGP
% calculate the upper area of CGP with different water height
A=9.245+19.85*pond/1000+9.47*pond^2/1000000-0.88*1.48;

end


function [ F_M,Cpp,tccc,tppp, T,FP,tee] = GA(j, Cp, i, ksat2, ksat3, psi, height,
delt_theta, tpp, tcc, f, QD)
% modified green ampt equation
%   j= time
%   Cp= C at j-1
%   i= water loading
%   ksat2= saturated infiltration rate, mm/h
%   ksat3= saturated infiltration rate, mm/min
%   psi= suction head
%   height= ponding water level at j-1
%   delt_theta= initial deficit
%   tpp= ponding time at j-1
%   tcc= ponding time at j-1
%   f= actual infiltration rate
%   QD= leakage/drainage


if i<ksat3 && height<=0
    Cpp=0;
else
    if Cp<=0
        Cpp=sum(i(1:j))-sum(QD(1:j-1))-ksat3*psi*delt_theta/(i-ksat3);
    else
        Cpp=Cp;
    end
```

```
end

T=(psi+height)*delt_theta/ksat2;
FP=sum(f(1:j-1))+ksat3*0.5-sum(QD(1:j-1))/4.289;

if Cp<=0 && Cpp>0 && tpp==0
    tppp= (j-1.5)/60;
else
    tppp=tpp;
end

if tppp==0
    tccc=0;
elseif tppp>0 && tcc<=0
    tccc= FP/ksat2-T*log(1+FP/((psi+height)*delt_theta));
else
    tccc=tcc;
end

tee=(j-1)/60-tppp+tccc;

if tee<0
    F_M=i;
else
    F_M=ksat2*(0.707*((tee+T)/tee)^0.5+0.667-0.236*(tee/(tee+T))^0.5-
0.138*(tee/(tee+T)))/60;
end

end


function [ Q_f, ieec,sqqqc,hee ] = CGPOVERFLOW( xx, yy, depth, h, he, iec,sqqc,
Q )
% varying area in the CGP
%   xx= the "2S+Q" in storage-outflow relationship
%   yy= the outflow in storage-outflow relationship
%   depth= ponding water level at t
%   h= threshold elevation
%    he= effective water level (above threshold) at t-1; hee= effective water
level (above threshold) at t
%   iec= water loading at t
%   sqqc= 2S-Q at t-1; sqqq= 2S-Q at t
%   Q= entering water

hee=depth-h;

if hee<=0
    ieec= 0;
elseif he<0
```

```
    ieec= max(0, Q-he*(AREA(h+he)+AREA(h))/2);   % subtract the filling volume
and infiltrated water
else
    ieec= max(0, Q);
end

I1= iec+ ieec;
SQQ1=I1+sqqc;

if hee<=0
    Q_f=0;
else
    Q_f=interp1(xx,yy,SQQ1,'pchip');  % interpolation for Q_f_overflow
end

sqqqc= SQQ1-2*Q_f;

%Q_f=max(0,Q_f);

end


function [ Qf, ieea,sqqq,effh ] = ALMAOVERFLOW( x, y, DEPTH, h00, effh1, iea,sqq,
ALMAsurface, iw, actinfil,Qo)
% constant area in ALMA
%   x= the "2S+Q" in storage-outflow relationship
%   y= the outflow in storage-outflow relationship
%   DEPTH= ponding water level at t
%   h00= threshold elevation
%   effh1= effective water level (above threshold) at t-1; hee= effective water
level (above threshold) at t
%   iea= water loading at t
%   sqq= 2S-Q at t-1; sqqq= 2S-Q at t
%   ALMAsurface= permeable area
%   iw= water loading at t
%   actinfil= actual infiltration rate at t
%   Qo= different overflow at t-1

effh=DEPTH-h00;

if effh<=0
    ieea= 0;
elseif effh1<0
    ieea= max(0, (iw-actinfil+effh1)*ALMAsurface-Qo);   % subtract the filling
volume and infiltrated water
else
    ieea= max(0, (iw-actinfil)*ALMAsurface-Qo);
end

I2= iea+ ieea;
```

```
SQQ=I2+sqq;

if effh<=0
    Qf=0;
else
    Qf=interp1(x,y,SQQ,'pchip');
end

sqqq= SQQ-2*Qf;

end


function [ af ] = ActualInfil( ksat3, d, pf, thick, A, p, e, theta, Qin,
Qdrain,SMAX,S,v)
% calculate the actual infiltration rate considering the change of effective
area in CGP
% ksat3= saturated infiltration rate, mm/min
% d= water level at t-1
% pf= potential infiltration rate at t
% thick= soil thickness
% A= permeable area
% p= porosity
% e= epsilon, calibration facor
% thera= water content at t-1
% Qin= entering water at t
% Qdrain= drainage at t-1
% smax= porosity
% s= storage in soil at t-1
% v= opening space,

pS=SMAX-S+Qdrain/A; % available storage in the soil

if d>0
    pH=Qin/A+d/v;
else
    pH=Qin/A;  % available standing water
end

if theta>=p
    af=min(ksat3*(1+d*e/thick),pH);
else
    af=min(min(pf,pH),pS);
end

end
```